

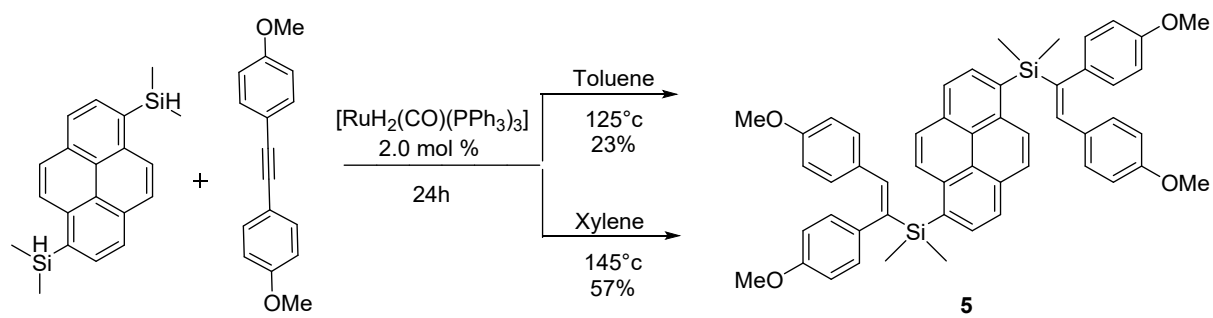
Supporting information for:

**Si-containing Polycyclic Aromatic Hydrocarbons: Synthesis and Opto-electronic Properties**

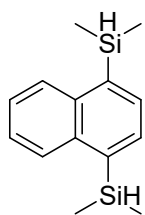
**Table of Content**

<b>Experimental part</b>	<b>page S2</b>
<b>NMR spectra</b>	<b>page S7</b>
<b>Crystallographic data and structure refinement parameters</b>	<b>Page S15</b>
<b>Optical properties</b>	<b>page S20</b>
<b>Electrochemical properties</b>	<b>page S22</b>
<b>Theoretical calculations</b>	<b>page S23</b>
<b>Thermal stability</b>	<b>page S26</b>
<b>Devices</b>	<b>page S26</b>

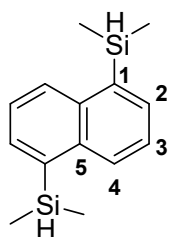
All experiments were performed under an atmosphere of dry argon using standard Schlenk techniques. Commercially available reagents were used as received without further purification. Solvents were freshly purified using MBRAUN SPS-800 drying columns. Separations were performed by gravity column chromatography on basic alumina (Aldrich, Type 5016A, 150 mesh, 58 Å) or silica gel (Merck Geduran 60, 0.063-0.200 mm).  $^1\text{H}$ ,  $^{13}\text{C}$ ,  $^{19}\text{F}$  and  $^{31}\text{P}$  NMR spectra were recorded on Bruker AV III 400 MHz NMR spectrometers equipped with BBFO probeheads. Assignment of H and C atoms is based on COSY, NOESY, edited-HSQC and HMBC experiments.  $^1\text{H}$  and  $^{13}\text{C}$  NMR chemical shifts were reported in parts per million (ppm) using residual solvent signal as reference. High-resolution mass spectra were obtained on a Varian MAT 311 or ZabSpec TOF Micromass instrument at Scanmat (UMS 2001). UV-Visible spectra were recorded at room temperature on a VARIAN Cary 5000 spectrophotometer. The UV-Vis emission and excitation spectra measurements were recorded on a FL 920 Edimburgh Instrument equipped with a Hamamatsu R5509-73 photomultiplier for the NIR domain (300-1700 nm) and corrected for the response of the photomultiplier. The absolute quantum yields (AQYs) were measured with a C9920-03 Hamamatsu system equipped with a 150 W xenon lamp, a monochromator, an integrating sphere. The electrochemical studies were carried out under argon using an Eco ChemieAutolab PGSTAT 30 potentiostat for cyclic voltammetry with the three-electrode configuration: the working electrode was a platinum disk, the reference electrode was a saturated calomel electrode and the counter-electrode a platinum wire. All potentials were internally referenced to the ferrocene/ferrocenium couple. For the measurements, concentrations of  $10^{-3}$  M of the electroactive species were used in freshly distilled and degassed dichloromethane and 0.2 M tetrabutylammoniumhexafluorophosphate. Thermogravimetric Analysis and Differential Scanning Calorimetry were performed by using a Mettler-Toledo TGA-DSC-1 apparatus under dry nitrogen flow at a heating rate of 10 °C/min.



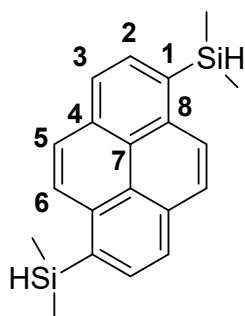
Scheme S1: Exemple of uncomplete cyclization



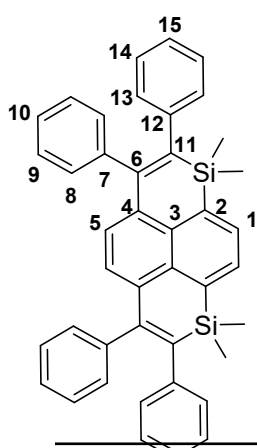
**1a.**<sup>1</sup> (*General method A*). 1,4-Dibromonaphthalene (1 g, 3.533 mmol, 1 eq) was degassed under argon and dissolved in 50 ml of dry Et<sub>2</sub>O. Then, the mixture was cooled to -78°C and tBuLi (7.0 mL, 10.6 mmol, 3 eq) was added dropwise. After 30 min at -78 ° C, the reaction was allowed to warm up to room temperature (RT). After 30 min the reaction is cooled to -78°C and Me<sub>2</sub>SiClH (3.6 mL, 35.33 mmol, 10 eq) was added dropwise and stirred at -78°C for 30 min and then at RT overnight. Then the organic phase was extracted with water, dried over MgSO<sub>4</sub> and the solvent evaporated. The product was purified through silica gel column chromatography (DCM/C<sub>7</sub> : 8/2). A colorless oil was obtained (855 mg, η = 99%). NMR data fit with previously reported procedure.



**1,5-bis(dimethylsilyl)naphthalene.** General method A was used with 1,5-Dibromonaphthalene (200 mg, 0.71 mmol, 1 eq), tBuLi (1.4 ml, 2.12 mmol, 3 eq), chlorodimethylsilane (0.72 ml, 7.07 mmol , 10 eq).The crude product was purified by column chromatography on silica gel with heptane, followed by precipitation by heptane-DCM mixtures. A colorless oil was obtained (150 mg, η = 87 %).<sup>1</sup>H NMR (400 MHz, CD<sub>2</sub>Cl<sub>2</sub>) δ 8.18 (d, *J* = 7.8 Hz, 2H, H<sub>2</sub>), 7.76 (d, *J* = 6.7 Hz, 2H, H<sub>4</sub>), 7.51 (t, *J* = 7.6 Hz, 2H, H<sub>3</sub>), 4.86 (hept, *J* = 3.8 Hz, 2H, H<sub>Si-H</sub>), 0.49 (d, *J* = 3.8 Hz, 12H, H<sub>CH<sub>3</sub></sub>). <sup>13</sup>C NMR (101 MHz, CD<sub>2</sub>Cl<sub>2</sub>) δ 137.2 (Cq), 137.1 (Cq), 133.8 (C<sub>4</sub>), 129.9 (C<sub>2</sub>), 125.6 (C<sub>3</sub>), -3.1 (C<sub>Me</sub>). 1 Cq is not observed due to overlap. HRMS (ASAP : 250°C) : [M+Na]<sup>+</sup> (C<sub>26</sub>H<sub>22</sub>NaSi<sub>2</sub>) : m/z Theoretical : 244.1098, m/z Found : 244.1097.



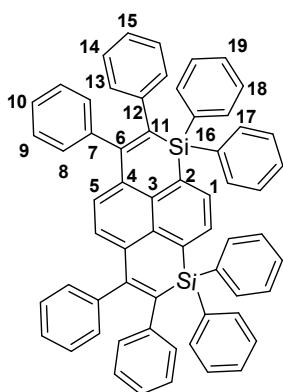
**1,6-bis(dimethylsilyl)pyrene.** General method A was used with 1,6-dibromopyrene (800 mg, 2.22 mmol, 1 eq), nBuLi (2.66 ml, 6.66 mmol, 3 eq), chlorodimethylsilane (1.00 ml, 8.88 mmol , 4 eq).The crude product was purified by column chromatography on silica gel with heptane, followed by precipitation by heptane-DCM mixtures. A white solid was obtained (443 mg, η = 63 %). <sup>1</sup>H NMR (400 MHz, CD<sub>2</sub>Cl<sub>2</sub>) δ 8.43 (d, *J* = 9.1 Hz, 2H, H<sub>2</sub>), 8.26 – 8.19 (m, 4H, H<sub>5,6</sub>), 8.14 (d, *J* = 9.1 Hz, 2H, H<sub>3</sub>), 5.09 (hept, *J* = 3.8 Hz, 2H, H<sub>Si-H</sub>), 0.62 (d, *J* = 3.8 Hz, 12H, H<sub>CH<sub>3</sub></sub>). <sup>13</sup>C NMR (101MHz, CDCl<sub>3</sub>): δ 136.2 (Cq), 133.7 (Cq), 132.7 (C<sub>5or6</sub>), 132.3 (Cq), 128.1 (C<sub>2</sub>), 127.9 (C<sub>3</sub>), 124.9 (Cq), 124.8 (C<sub>5or6</sub>), -2.8 (C<sub>CH<sub>3</sub></sub>). HRMS (ESI, CH<sub>3</sub>OH / CH<sub>2</sub>Cl<sub>2</sub> : 9/1) [M+Na]<sup>+</sup> (C<sub>26</sub>H<sub>22</sub>NaSi<sub>2</sub>) : m/z Theoretical : 341.1152, m/z Found : 341.1149.



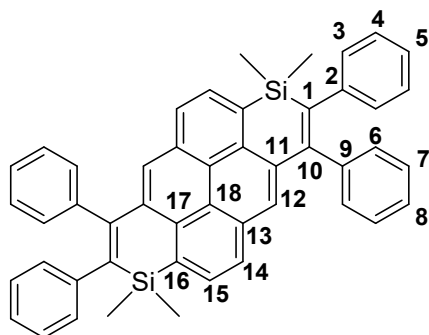
**2a.** (*General method B*).In a Ar purged shlenk, [RuH<sub>2</sub>(CO)(PPh<sub>3</sub>)<sub>3</sub>] (0.147 mg, 0.16 mmol, 0.08 eq), **1a** (500 mg, 2.05 mmol, 1 eq) and diphenylacetylene (1.458 g, 8.18 mmol, 4 eq) were dissolved in 4.5 mL of dry toluene. The reaction mixture was stirred at 125 °C for 24 h. The solvent was evaporated. The crude was subjected to column chromatography on silica gel with (heptane / DCM 9:1), a yellowish solid was obtained (260 mg, η = 22 %). <sup>1</sup>H NMR (300 MHz, CD<sub>2</sub>Cl<sub>2</sub>) δ 8.01 (s, 2H, H<sub>1</sub>), 7.19 – 7.08 (m, 10H, H<sub>9, 14,15</sub>), 7.07 – 7.01 (m, 6H, H<sub>8, 10</sub>), 6.98 – 6.93 (m, 4H, H<sub>13</sub>), 6.91 (s, 2H, H<sub>5</sub>), 0.41 (s, 12H, H<sub>CH<sub>3</sub></sub>). <sup>13</sup>C NMR (75 MHz, CD<sub>2</sub>Cl<sub>2</sub>) δ 152.3 (s, Cq), 143.5 (s, Cq), 143.3 (s, Cq), 142.4 (s, Cq), 136.7 (s, Cq), 136.66 (s, Cq), 134.32 (s, Cq), 133.11 (s, C<sub>1</sub>), 131.12 (s, C<sub>5</sub>), 130.95 (s, C<sub>8</sub>), 128.8 (s, C<sub>13</sub>), 128.1 (s, C<sub>14</sub>), 128.0 (s, C<sub>9</sub>), 126.5 (s,

<sup>1</sup> H. Maeda, T. Maeda and K. Mizuno, *Molecules*, **2012**, *17*, 5108–5125

C<sub>15</sub>), 125.4 (s, C<sub>10</sub>), -0.1 (s, C<sub>CH3</sub>). HRMS (ESI, CH<sub>3</sub>OH / CH<sub>2</sub>Cl<sub>2</sub> : 9/1) [M+K]<sup>+</sup> (C<sub>42</sub>H<sub>36</sub>Si<sub>2</sub>K) : m/z Theoretical : 635.1987, m/z Found : 635.1988.

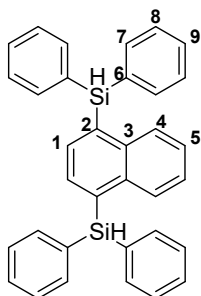


3. General method B was used with compound 1,5-bis(dimethylsilyl)naphthalene (150 mg, 0.61 mmol, 1 eq). [RuH<sub>2</sub>(CO)(PPh<sub>3</sub>)<sub>3</sub>] complex (45 mg, 0.05 mmol, 0.08 eq), diphenylacetylene (440 mg, 2.45 mmol, 4 eq) and 1.5 ml of toluene. The crude product was purified by column chromatography on silica gel (gradient of heptane/DCM from 8:2 to 1:1). A white solid was obtained. (125 mg, η = 34 %). <sup>1</sup>H NMR (400 MHz, CD<sub>2</sub>Cl<sub>2</sub>) δ 7.88 (s, 2H, H<sub>1</sub>), 7.59 – 7.54 (m, 8H, H<sub>17</sub>), 7.42 – 7.36 (m, 4H, H<sub>19</sub>), 7.35 – 7.29 (m, 8H, H<sub>18</sub>), 7.18 – 7.13 (m, 4H, H<sub>14</sub>), 7.12 – 7.06 (m, 8H, H<sub>5,8,15</sub>), 6.91 – 6.83 (m, 6H, H<sub>9,10</sub>), 6.71 – 6.66 (m, 4H, H<sub>13</sub>). <sup>13</sup>C NMR (101 MHz, CD<sub>2</sub>Cl<sub>2</sub>) δ 154.7 (s, Cq), 142.6 (s, Cq), 142.1 (s, Cq), 139.9 (s, Cq), 136.7 (s, C<sub>17</sub>), 136.7 (s, Cq), 135.2 (s, C<sub>1</sub>), 134.5 (s, C<sub>16</sub>), 134.5 (s, Cq), 133.7 (s, Cq), 131.8 (s, C<sub>5</sub>), 131.0 (s, C<sub>8</sub>), 130.1 (s, C<sub>19</sub>), 129.5 (s, C<sub>13</sub>), 128.3 (s, C<sub>18</sub>), 127.9 (s, C<sub>9</sub>), 127.5 (s, C<sub>14</sub>), 126.6 (s, C<sub>10</sub>), 125.3 (s, C<sub>15</sub>). HRMS (ESI, CH<sub>3</sub>OH/CH<sub>2</sub>Cl<sub>2</sub> : 9/1) [M+Na]<sup>+</sup> (C<sub>62</sub>H<sub>44</sub>NaSi<sub>2</sub>) : m/z Theoretical : 867.2874, m/z Found : 867.2875.

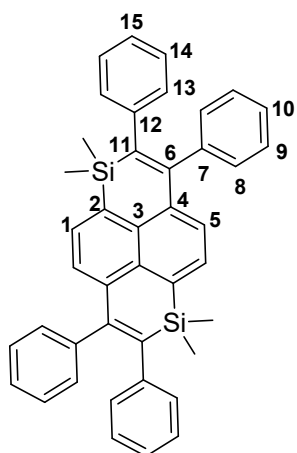


4. General method B was used with compound 1,6-bis(dimethylsilyl)pyrene (200 mg, 0.628 mmol, 1 eq). [RuH<sub>2</sub>(CO)(PPh<sub>3</sub>)<sub>3</sub>] (46 mg, 0.05 mmol, 0.08 eq), diphenylacetylene (447 mg, 2.51 mmol, 4 eq) and 1 ml of toluene. The crude product was purified by column chromatography on silica gel (gradient of heptane/DCM from 8:2 to 1:1). A white solid was obtained. (110 mg, η = 26 %). <sup>1</sup>H NMR (400 MHz, CD<sub>2</sub>Cl<sub>2</sub>) δ 8.20 (d, J = 7.5 Hz, 2H, H<sub>15</sub>), 7.97 (d, J = 7.5 Hz, 2H, H<sub>14</sub>), 7.77 (s, 2H, H<sub>12</sub>), 7.31 – 7.25 (m, 4H, H<sub>4</sub>), 7.25 –

7.19 (m, 6H, H<sub>3,5</sub>), 7.18 – 7.12 (m, 4H, H<sub>7</sub>), 7.06 – 7.00 (m, 2H, H<sub>8</sub>), 7.00 – 6.95 (m, 4H, H<sub>6</sub>), 0.41 (s, 12H, H<sub>CH3</sub>). <sup>13</sup>C NMR (101 MHz, CD<sub>2</sub>Cl<sub>2</sub>) δ 152.1 (Cq), 144.0 (Cq), 143.4 (Cq), 142.1 (Cq), 135.4 (Cq), 134.0 (C<sub>12</sub>), 132.9 (Cq), 132.3 (Cq), 132.2 (C<sub>15</sub>), 131.1 (C<sub>3</sub>), 128.8 (C<sub>6</sub>), 128.0 (C<sub>4</sub>), 128.0 (C<sub>7</sub>), 126.6 (C<sub>5</sub>), 126.5 (C<sub>14</sub>), 125.3 (C<sub>8</sub>), 124.6 (Cq), -0.4 (C<sub>CH3</sub>). One <sup>13</sup>C is missing due to overlap. HRMS (ESI, CH<sub>3</sub>OH/CH<sub>2</sub>Cl<sub>2</sub> : 9/1) [M+Na]<sup>+</sup> (C<sub>48</sub>H<sub>38</sub>NaSi<sub>2</sub>) : m/z Theoretical : 693.2404, m/z Found : 693.2408.

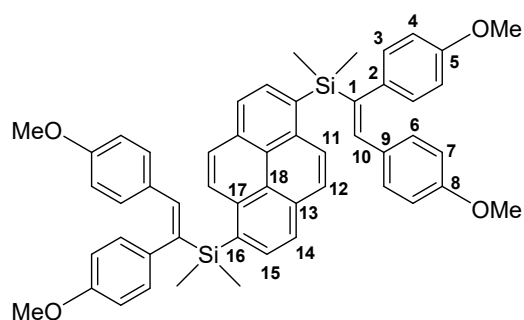


**1,4-bis(diphenylsilyl)naphthalene**. General method A was used with 1,4-Dibromonaphthalene (400 mg, 1.389 mmol, 1 eq), n-BuLi (1.82 ml, 4.196 mmol, 3 eq), chlorodiphenylsilane (1.09 ml, 5.556 mmol, 4 eq). The crude product was purified by column chromatography on silica gel with heptane, followed by precipitation by heptane-DCM mixtures. A white solid was obtained (280 mg, η = 41 %). <sup>1</sup>H NMR (400 MHz, CD<sub>2</sub>Cl<sub>2</sub>) δ 8.11 (dd, J = 6.3, 3.4 Hz, 2H, H<sub>4</sub>), 7.60 – 7.55 (m, 10H, H<sub>1,7</sub>), 7.46 – 7.33 (m, 14H, H<sub>5,8,9</sub>), 5.89 (s, 2H, H<sub>Si-H</sub>). <sup>13</sup>C NMR (101 MHz, CD<sub>2</sub>Cl<sub>2</sub>) δ 137.4 (Cq), 136.3 (C<sub>7</sub>), 135.1 (Cq), 134.6 (C<sub>1</sub>), 133.4 (Cq), 130.3 (C<sub>9</sub>), 129.4 (C<sub>4</sub>), 128.5 (C<sub>8</sub>), 126.3 (C<sub>5</sub>). HRMS (ASAP : 225 °C) : M<sup>+</sup> (C<sub>34</sub>H<sub>28</sub>Si<sub>2</sub>) : m/z Theoretical : 492.1724 m/z Found : 492.1719.



: 619.2248, m/z Found : 619.2251.

**2b.** General method B was used with 1,5-bis(dimethylsilyl)naphthalene (150 mg, 0.61 mmol, 1 eq).  $[\text{RuH}_2(\text{CO})(\text{PPh}_3)_3]$  complex (45 mg, 0.05 mmol, 0.08 eq), diphenylacetylene (440 mg, 2.45 mmol, 4 eq) and 1.5 ml of toluene. The crude product was purified by column chromatography on silica gel (gradient of heptane/DCM from 8:2 to 1:1). A white solid was obtained. (125 mg,  $\eta = 34\%$ ).  $^1\text{H}$  NMR (400 MHz,  $\text{CD}_2\text{Cl}_2$ )  $\delta$  7.70 (d,  $J = 7.4$  Hz, 2H,  $\text{H}_1$ ), 7.25 – 7.19 (m, 6H,  $\text{H}_{5,14}$ ), 7.18 – 7.10 (m, 10H,  $\text{H}_{8,9,15}$ ), 7.06 – 7.01 (m, 2H,  $\text{H}_{10}$ ), 6.94 (d,  $J = 6.7$  Hz, 4H,  $\text{H}_{13}$ ), 0.33 (s, 12H,  $\text{H}_{\text{CH}_3}$ ).  $^{13}\text{C}$  NMR (75 MHz,  $\text{CD}_2\text{Cl}_2$ )  $\delta$  152.3 (s, Cq), 143.1 (s, Cq), 143.0 (s, Cq), 142.2 (s, Cq), 137.4 (s, Cq), 135.1 (s, Cq), 133.7 (s, Cq), 133.4 (s,  $\text{C}_1$ ), 130.5 (s,  $\text{C}_8$ ), 129.7 (s,  $\text{C}_5$ ), 128.2 (s,  $\text{C}_{13}$ ), 127.5 (s,  $\text{C}_{14}$ ), 127.5 (s,  $\text{C}_9$ ), 126.0 (s,  $\text{C}_{15}$ ), 124.7 (s,  $\text{C}_{10}$ ), -0.9 (s,  $\text{C}_{\text{CH}_3}$ ). HRMS (ESI,  $\text{CH}_3\text{OH}/\text{CH}_2\text{Cl}_2$ : 9/1)  $[\text{M}+\text{Na}]^+$  ( $\text{C}_{42}\text{H}_{36}\text{NaSi}_2$ ): m/z Theoretical



**5:** General method B was used with compound 1,6-bis(dimethylsilyl)pyrene (100 mg, 0.31 mmol, 1eq).  $\text{RuH}_2(\text{CO})(\text{PPh}_3)_3$  (4.0 mol%), Bis-(4-methoxyphenyl)acetylene (295 mg, 1.24 mmol, 4eq) and 1 ml of xylene. The mixture was heated to  $140^\circ\text{C}$  during 20h. The crude product was purified by column chromatography on silica gel (gradient of heptane/DCM from 1:1 to DCM). A solid was obtained. (172 mg,  $\eta = 57\%$ ).  $^1\text{H}$  NMR (300 MHz,  $\text{CD}_2\text{Cl}_2$ )  $\delta$  8.26 (d,  $J = 9.1$  Hz, 2H,  $\text{H}_{15}$ ), 8.23 (d,  $J = 7.6$  Hz, 2H,  $\text{H}_{11}$ ), 8.11 (d,  $J = 7.7$  Hz, 2H,  $\text{H}_{12}$ ), 8.02 (d,  $J = 9.2$  Hz, 2H,  $\text{H}_{14}$ ), 7.39 (s, 2H,  $\text{H}_{10}$ ), 7.32 (d,  $J = 8.7$  Hz, 4H,  $\text{H}_3$ ), 6.94 (d,  $J = 8.6$  Hz, 4H,  $\text{H}_7$ ), 6.87 (d,  $J = 8.7$  Hz, 4H,  $\text{H}_4$ ), 6.30 (d,  $J = 8.7$  Hz, 4H,  $\text{H}_6$ ), 3.78 (s, 6H,  $\text{H}_{\text{OMe}}$ ), 3.47 (s, 6H,  $\text{H}_{\text{OMe}}$ ), 0.50 (s, 12H,  $\text{H}_{\text{SiMe}}$ ).  $^{13}\text{C}$  NMR (75 MHz,  $\text{CD}_2\text{Cl}_2$ )  $\delta$  158.5, 158.1, 146.1 (CH), 143.3, 139.3, 135.2, 132.6 (CH), 131.4, 131.3, 129.5 (CH), 128.8 (CH), 128.3 (CH), 126.7 (CH), 124.5, 124.1 (CH), 114.0, 113.4 (CH), 112.5 (CH), 55.1 ( $\text{C}_{\text{OMe}}$ ), 54.8 ( $\text{C}_{\text{OMe}}$ ), 0.8 ( $\text{C}_{\text{SiMe}}$ ). HRMS (ESI,  $\text{CH}_3\text{OH}/\text{CH}_2\text{Cl}_2$ : 9/1)  $[\text{M}+\text{Na}]^+$  ( $\text{C}_{52}\text{H}_{50}\text{O}_4\text{NaSi}_2$ ) m/z Theoretical : 817.3140, m/z Found : 817.3143.

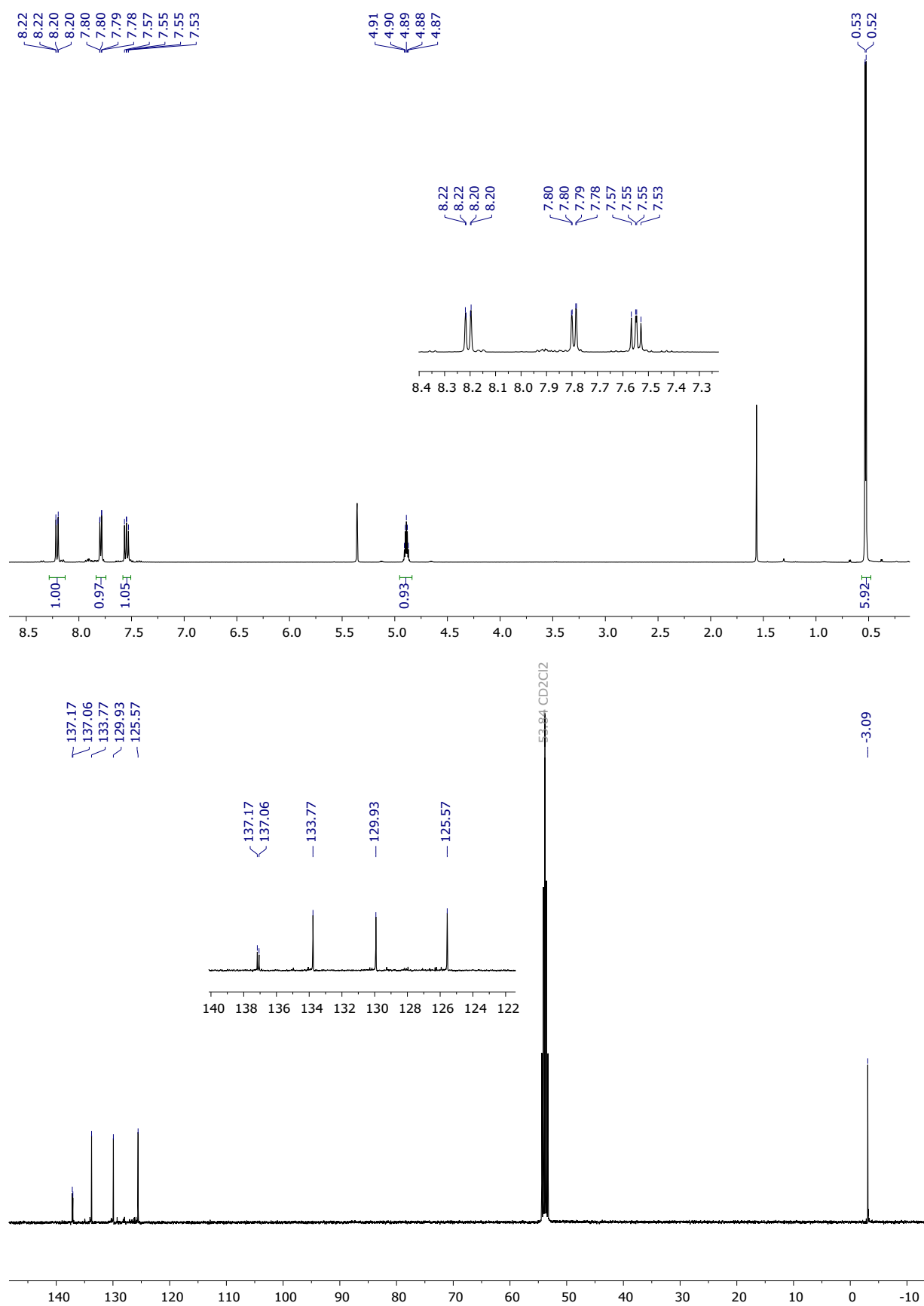


Figure S1: <sup>1</sup>H NMR (400 MHz, CD<sub>2</sub>Cl<sub>2</sub>) and <sup>13</sup>C NMR (101 MHz, CD<sub>2</sub>Cl<sub>2</sub>), spectra of compound 1,5-bis(dimethylsilyl)naphthalene.

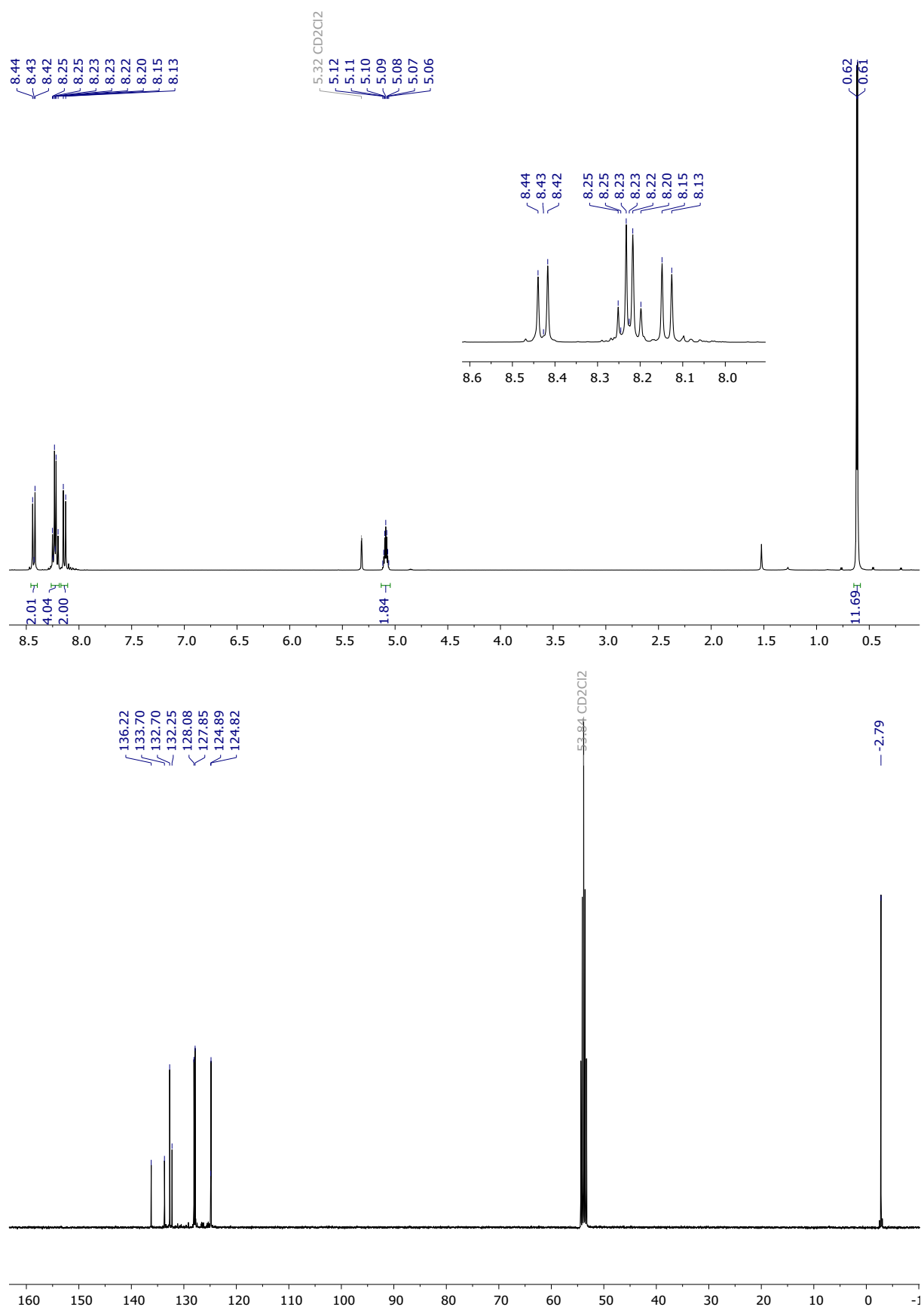


Figure S2: <sup>1</sup>H NMR (400 MHz, CD<sub>2</sub>Cl<sub>2</sub>) and <sup>13</sup>C NMR (101 MHz, CD<sub>2</sub>Cl<sub>2</sub>), spectra of compound **1,6-bis(dimethylsilyl)pyrene**.



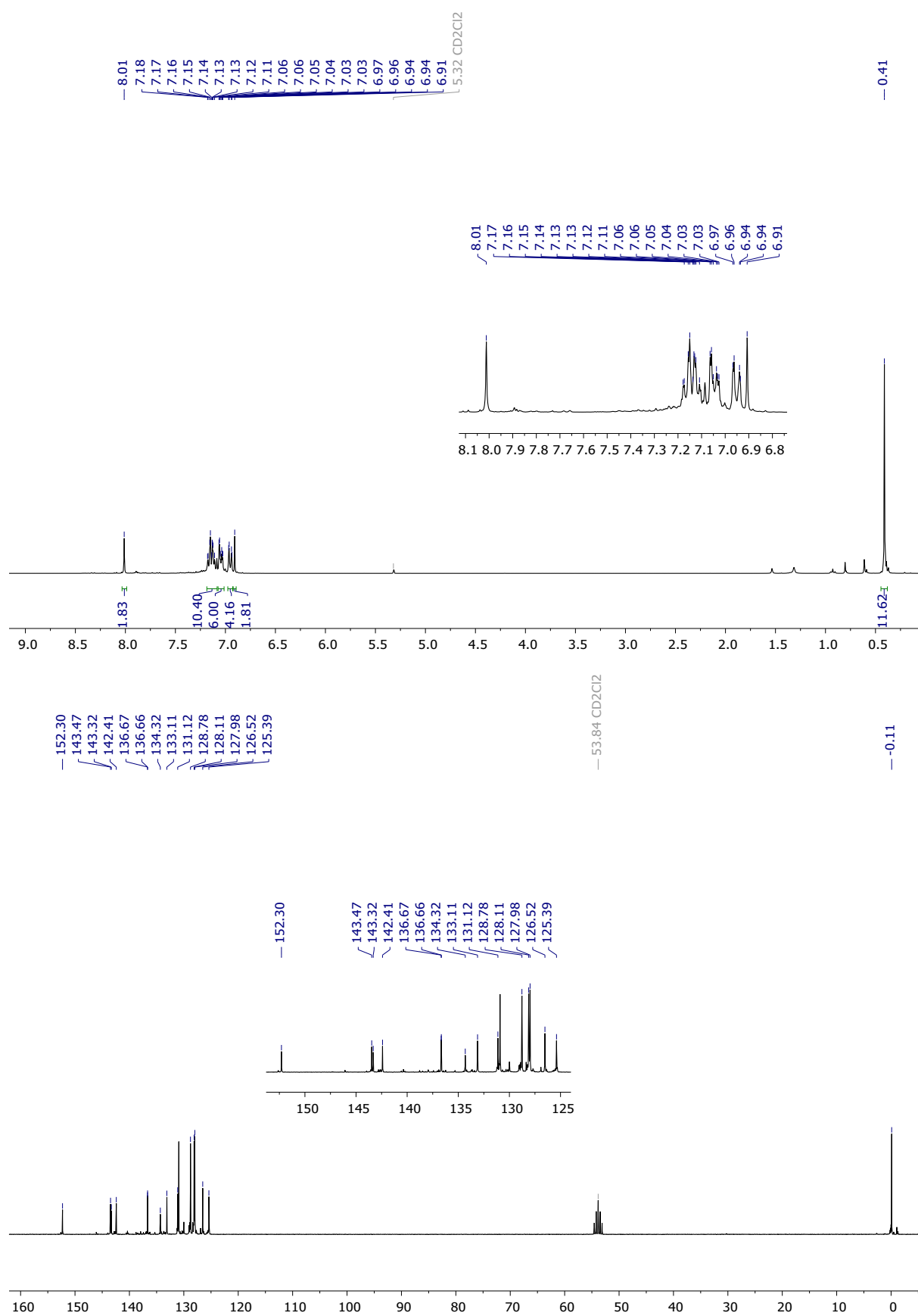


Figure S3: <sup>1</sup>H NMR (300 MHz, CD<sub>2</sub>Cl<sub>2</sub>) and <sup>13</sup>C NMR (75 MHz, CD<sub>2</sub>Cl<sub>2</sub>), spectra of compound **2a**.

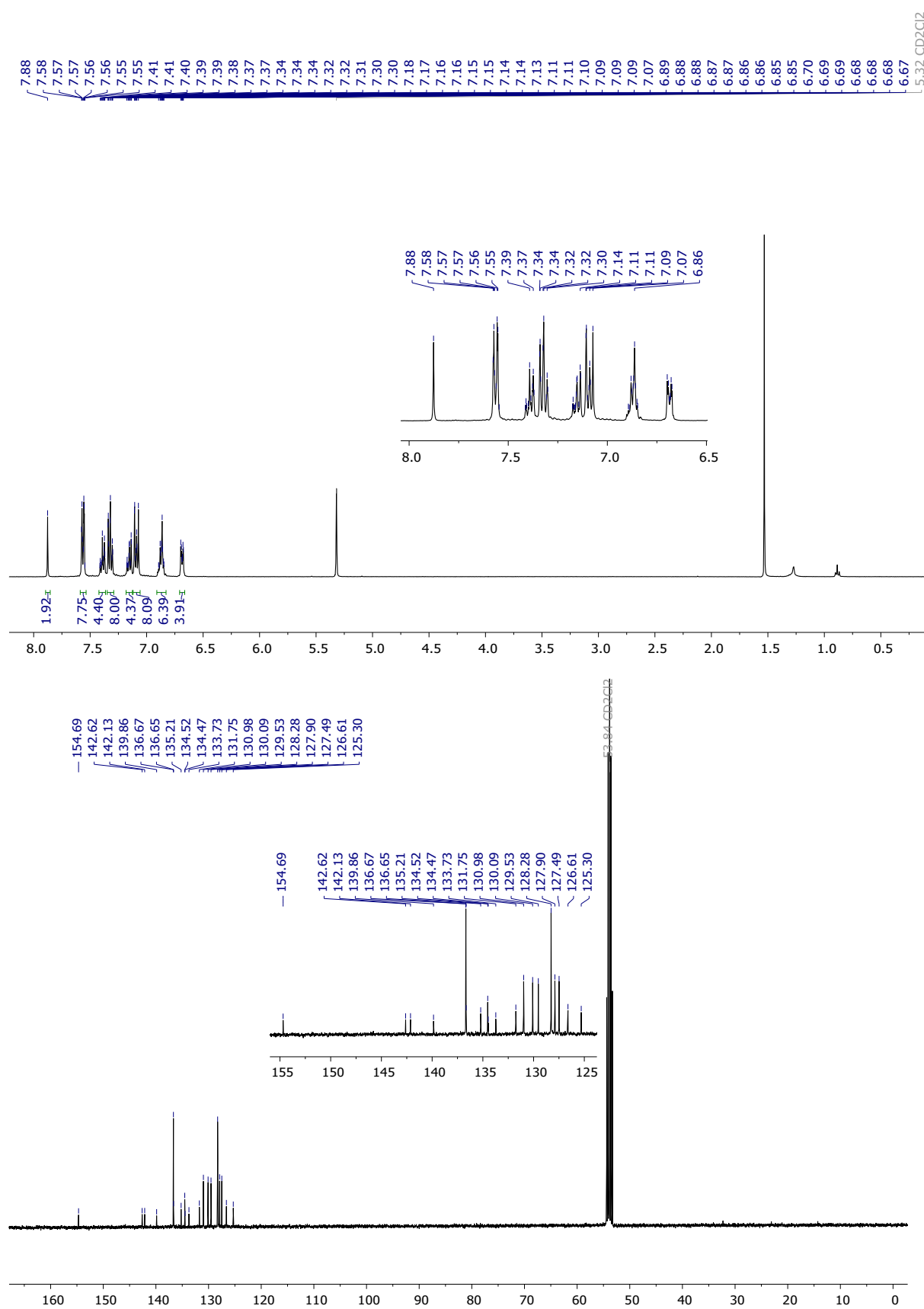


Figure S4: <sup>1</sup>H NMR (400 MHz, CD<sub>2</sub>Cl<sub>2</sub>) and <sup>13</sup>C NMR (75 MHz, CD<sub>2</sub>Cl<sub>2</sub>), spectra of compound **3**.

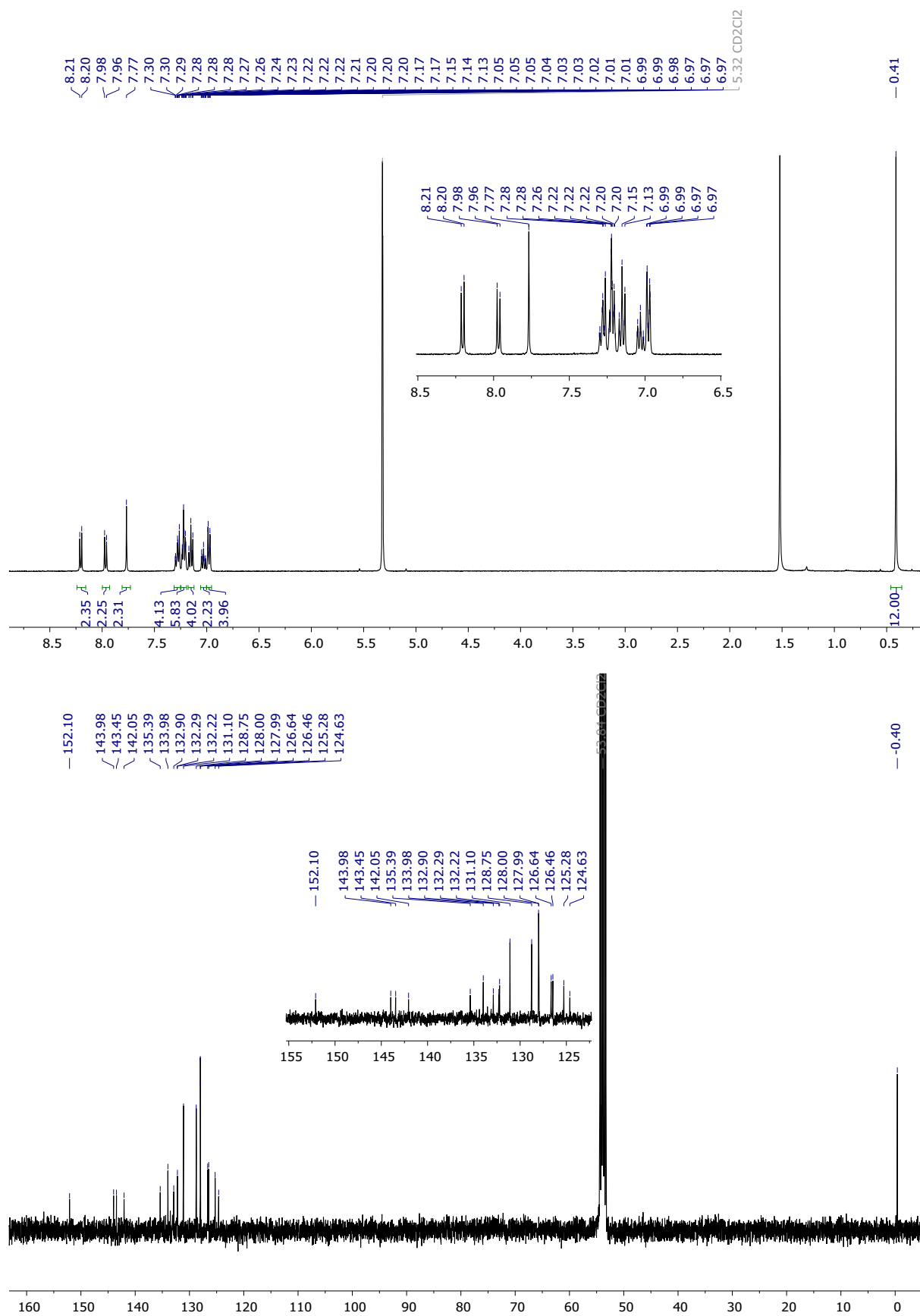


Figure S5: <sup>1</sup>H NMR (400 MHz, CD<sub>2</sub>Cl<sub>2</sub>) and <sup>13</sup>C NMR (101 MHz, CD<sub>2</sub>Cl<sub>2</sub>), spectra of compound 4.

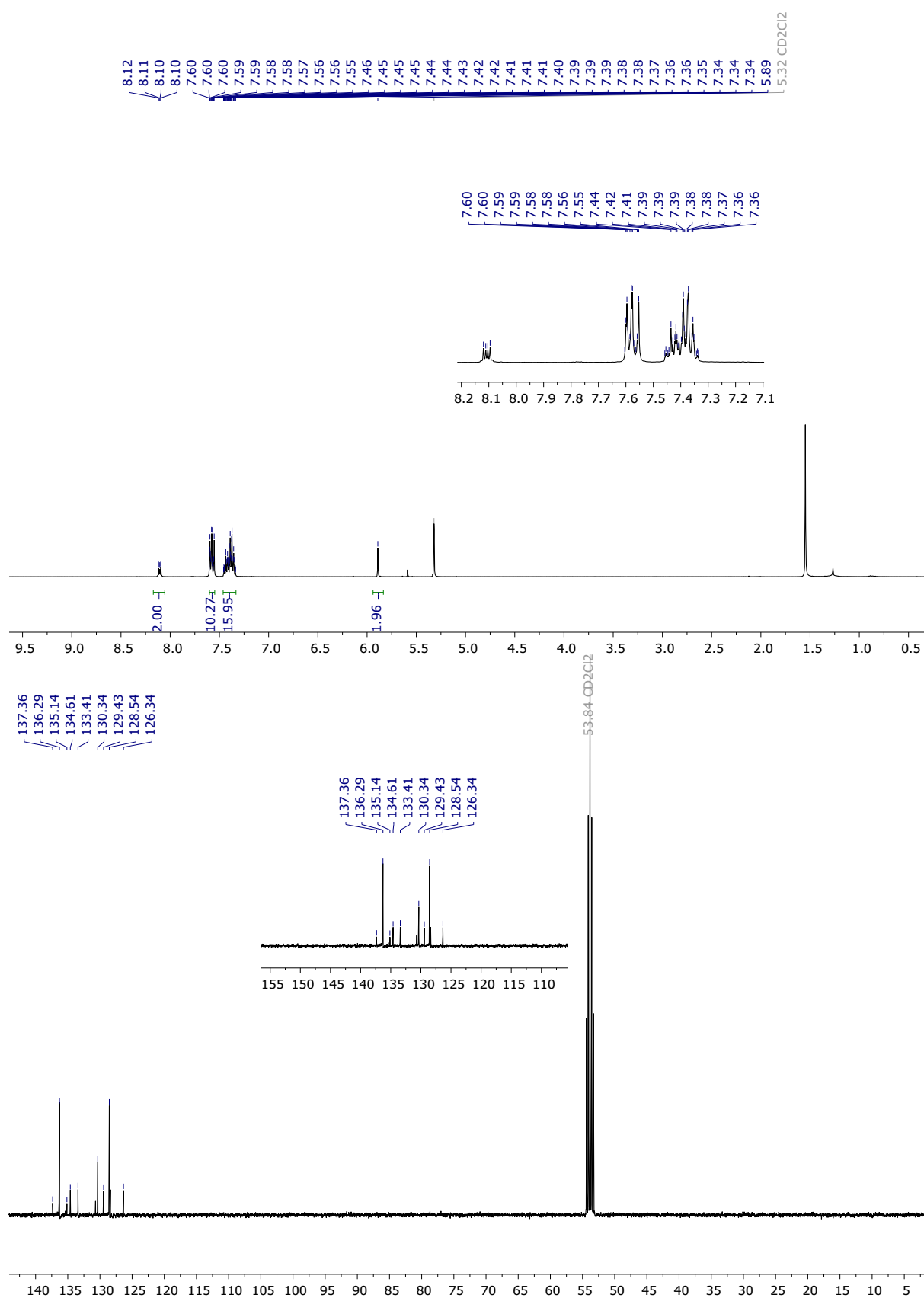


Figure S6: <sup>1</sup>H NMR (400 MHz, CD<sub>2</sub>Cl<sub>2</sub>) and <sup>13</sup>C NMR (101 MHz, CD<sub>2</sub>Cl<sub>2</sub>), spectra of compound 1,4-bis(diphenylsilyl)naphthalene .

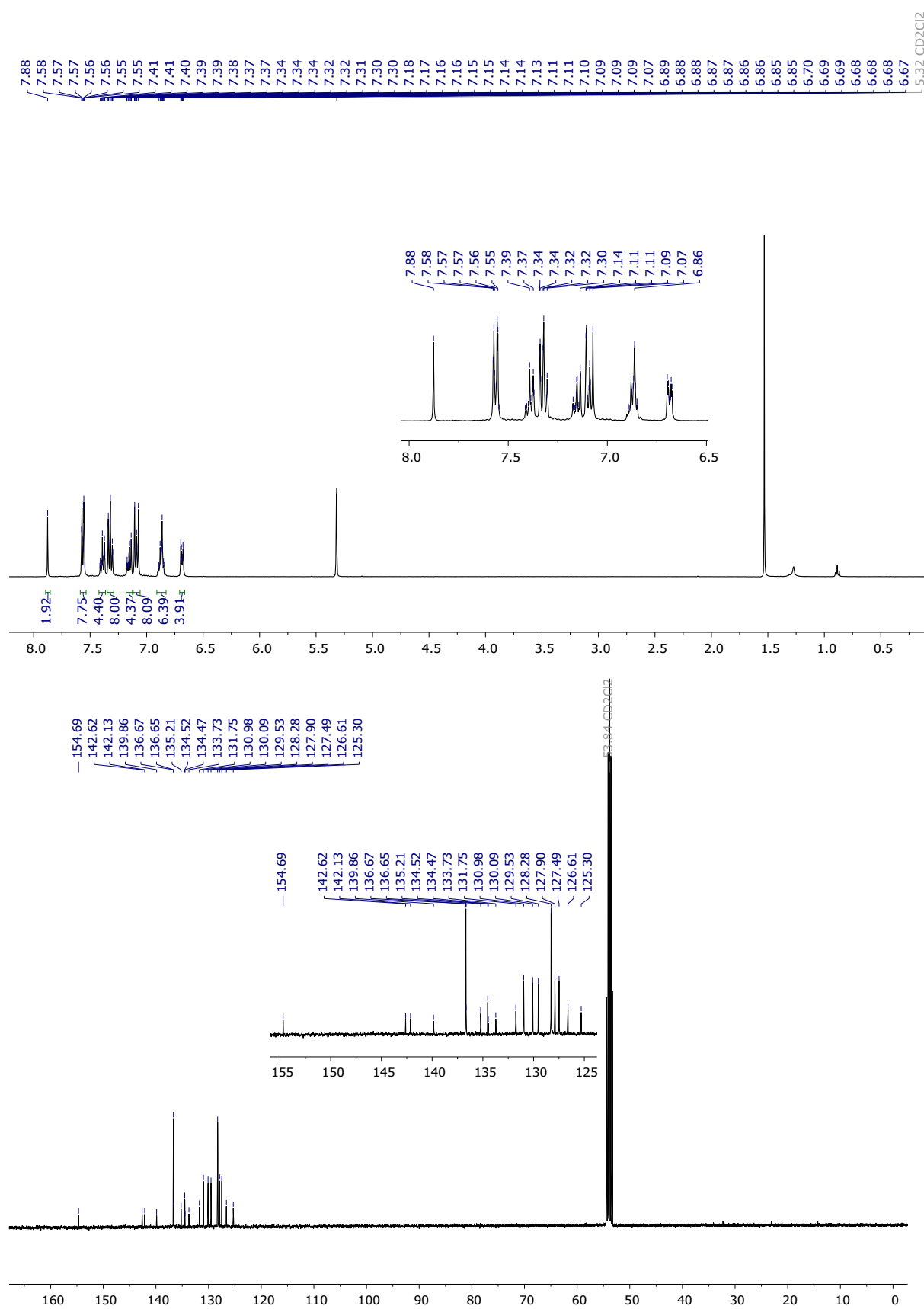


Figure S7: <sup>1</sup>H NMR (400 MHz, CD<sub>2</sub>Cl<sub>2</sub>) and <sup>13</sup>C NMR (101 MHz, CD<sub>2</sub>Cl<sub>2</sub>), spectra of compound **2b**.

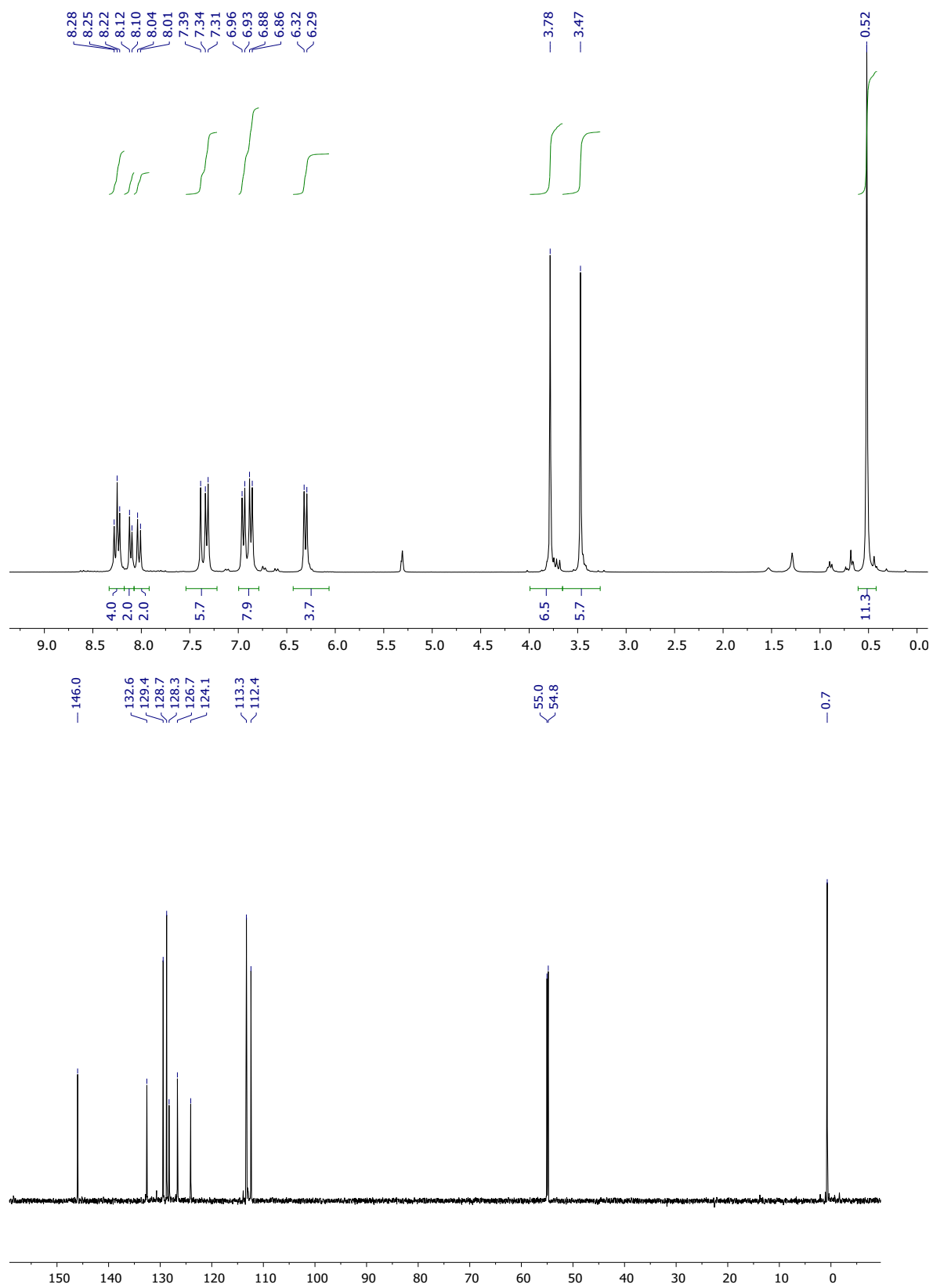


Figure S8:  $^1\text{H}$  NMR (400 MHz,  $\text{CD}_2\text{Cl}_2$ ) and  $^{13}\text{C}$  NMR (101 MHz,  $\text{CD}_2\text{Cl}_2$ ), spectra of compound **5**.

## X-ray crystallography

Single crystals suitable for X-Ray crystal analysis were obtained by slow diffusion of vapors of pentane into a dichloromethane solution of the derivatives at rt. Single crystal data collection were performed at 150 K with an D8 VENTURE Bruker AXS diffractometer equipped with a (CMOS) PHOTON 100 detector with Mo- $K\alpha$  radiation ( $\lambda = 0.71073 \text{ \AA}$ ). The structure was solved by dual-space algorithm using the *SHELXT* program<sup>2</sup>, and then refined with full-matrix least-squares methods based on  $F^2$  (*SHELXL*).<sup>3</sup>

All non-hydrogen atoms were refined with anisotropic atomic displacement parameters. H atoms were finally included in their calculated positions and treated as riding on their parent atom with constrained thermal parameters.

---

<sup>2</sup> G. M. Sheldrick, *Acta Cryst.*, **2015**, A71, 3-8

<sup>3</sup>G. M. Sheldrick, *Acta Cryst.*, **2015**, C71, 3-8

Table S1: Crystallographic data

Compound	2a	2b	4	5
CCDC	1982459	1982458	1982457	2001027
Formula	C42 H36 Si2	C62 H44 Si2	C50 H42 Cl4 Si2	C <sub>52</sub> H <sub>50</sub> O <sub>4</sub> Si <sub>2</sub>
MW	596.89	845.15	840.81	795.10
a (Å)	18.495(2)	12.7200(11)	14.192(2)	11.9542(16)
b (Å)	6.5338(8)	14.7321(13)	8.8346(14)	9.7509(12)
c (Å)	28.922(3)	15.2928(12)	17.444(2)	18.570(2)
α (°)	90	71.598(3)	90	90
β (°)	99.125(4)	66.440(3)	96.424(6)	106.220(4)
γ (°)	90	73.259(3)	90	90
V (Å <sup>3</sup> )	3450.8(7)	2449.0(4)	2173.4(5)	2078.4(4)
Z	4	2	2	2
D <sub>c</sub> (g.cm <sup>-3</sup> )	1.149	1.146	1.285	1.270
Crystal system	monoclinic	triclinic	monoclinic	monoclinic
Space group	P 2 <sub>1</sub> /c	P -1	P 2 <sub>1</sub> /n	P 2 <sub>1</sub> /c
T (K)	293	150	150	150
λ, Mo-Kα (Å)	0.71073	0.71073	0.71073	0.71073
μ (mm <sup>-1</sup> )	0.130	0.111	0.362	0.133
F(000)	1264	888	876	844
θ limit (°)	3.198 to 27.482	2.092 to 27.529	2.350 to 27.510	2.284 to 27.511
Index ranges <i>hkl</i>	-24 ≤ h ≤ 24	-16 ≤ h ≤ 16	-18 ≤ h ≤ 18	-15 ≤ h ≤ 15
	-8 ≤ k ≤ 8	-19 ≤ k ≤ 19	-10 ≤ k ≤ 11	-12 ≤ k ≤ 11
	-36 ≤ l ≤ 37	-19 ≤ l ≤ 17	-22 ≤ l ≤ 22	-23 ≤ l ≤ 24
Reflections collected	33897	46719	18903	17466
Indep. reflections	7687	11215	4985	4740
Reflections [ <i>I</i> > 2σ( <i>I</i> )]	6171	9181	4158	3969
Data / restraints / parameters	7687 / 0 / 401	11215 / 0 / 577	4985 / 0 / 253	4740 / 0 / 266
Goodness-of-fit on <i>F</i> <sup>2</sup>	1.094	1.024	1.052	1.048
Final <i>R</i> indices [ <i>I</i> > 2σ( <i>I</i> )]	R1 = 0.0652	R1 = 0.0461	R1 = 0.0828	R1 = 0.0565
	wR2 = 0.1404	wR2 = 0.1212	wR2 = 0.2151	wR2 = 0.1485
<i>R</i> indices (all data)	R1 = 0.0830	R1 = 0.0592	R1 = 0.0940	R1 = 0.0677
	wR2 = 0.1488	wR2 = 0.1325	wR2 = 0.2318	wR2 = 0.1608
Largest diff peak and hole (e Å <sup>-3</sup> )	0.265 and -0.249	0.363 and -0.719	1.235 and -1.033	0.534 and -0.597



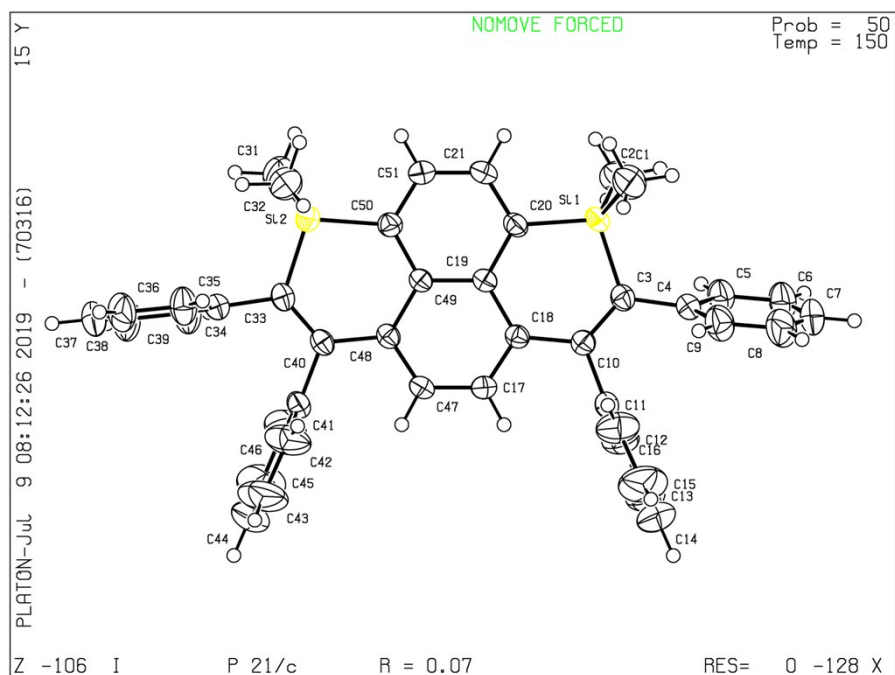


Figure S9: ORTEP representation of **2a** with 50% probability ellipsoids

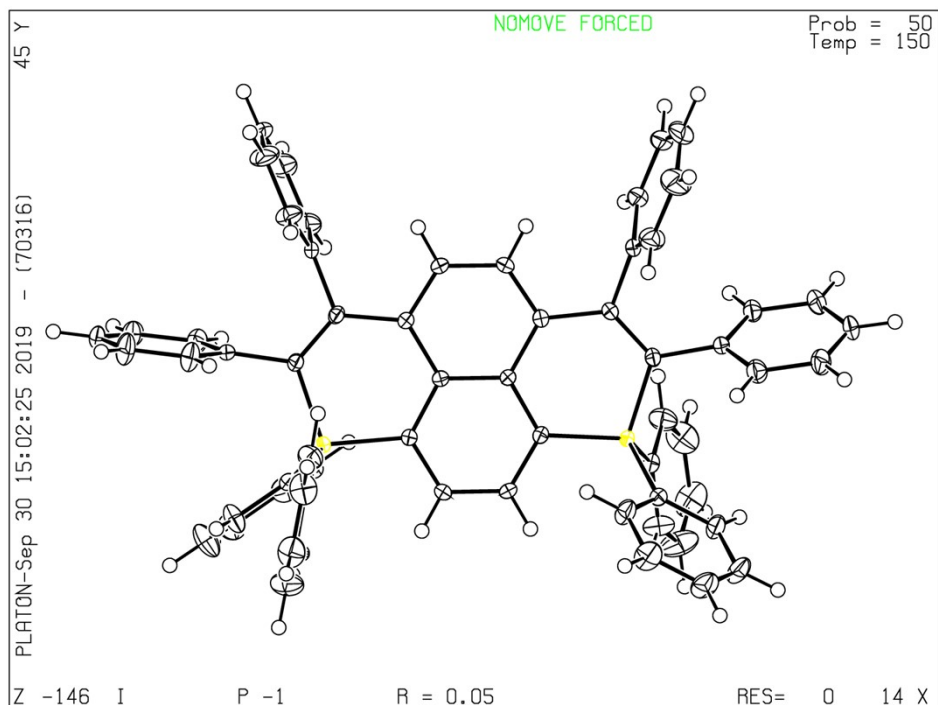


Figure S10: ORTEP representation of **2b** with 50% probability ellipsoids

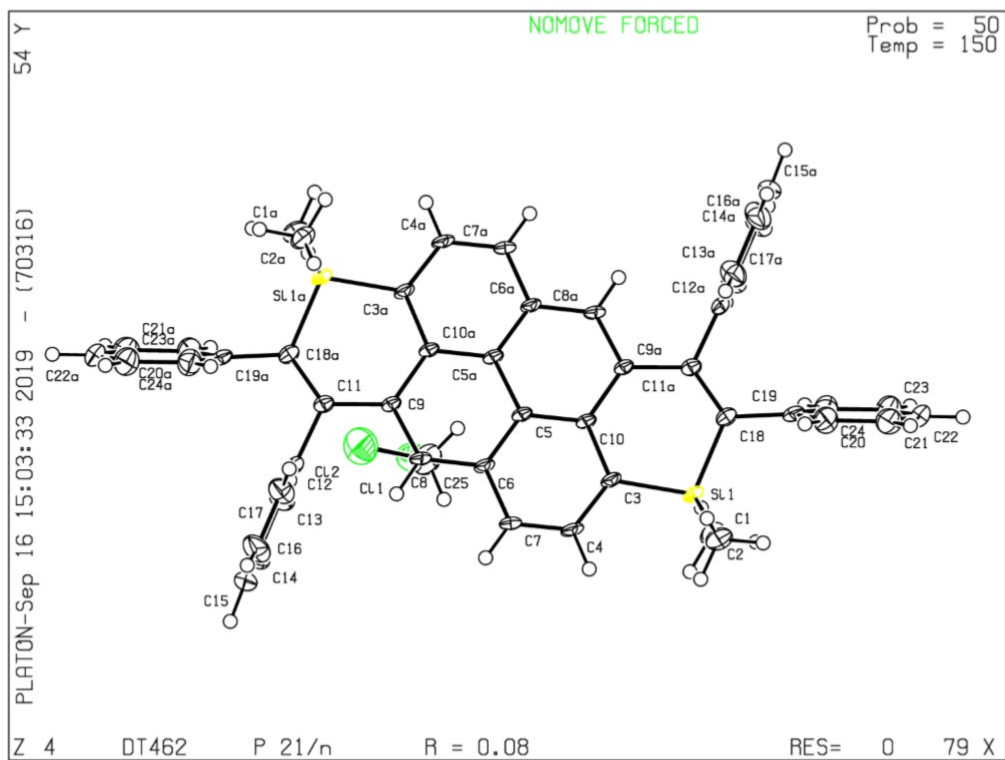


Figure S11: ORTEP representation of **4** with 50% probability ellipsoids

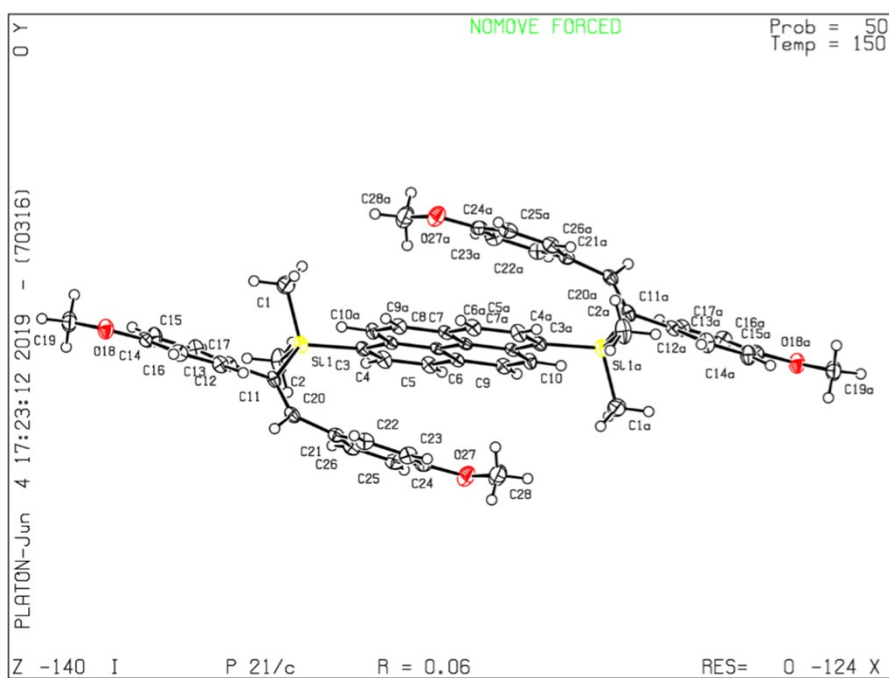
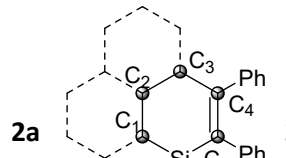


Figure S12: ORTEP representation of **5** with 50% probability ellipsoids

Table S2. Crystallographic distances



	<b>2a</b>	<b>2b</b>	<b>3</b>	<b>4</b>
<b>Si-C<sub>1</sub></b> (Å)	1.851(3)/1.860(3)	1.862(2)/1.865(2)	1.858(2)	1.858(3)
<b>Si-C<sub>5</sub></b> (Å)	1.853(3)/1.853(2)	1.860(2)/1.856(1)	1.855(2)	1.859(2)
<b>C<sub>1</sub>-C<sub>2</sub></b> (Å)	1.428(3)/1.432(3)	1.426(2)/1.429(2)	1.433(2)	1.418(3)
<b>C<sub>2</sub>-C<sub>3</sub></b> (Å)	1.458(3)/1.456(3)	1.453(2)/1.449(2)	1.450(2)	1.469(3)
<b>C<sub>3</sub>-C<sub>4</sub></b> (Å)	1.491(3)/1.491(3)	1.498(2)/1.494(2)	1.501(2)	1.496(4)
<b>C<sub>4</sub>-C<sub>5</sub></b> (Å)	1.353(3)/1.358(3)	1.359(2)/1.352(3)	1.357(2)	1.352(3)
<b>C<sub>1</sub>-Si-C<sub>5</sub></b> (°)	104.00(1)/103.30(1)	103.87(8)/103.77(2)	103.20(7)	103.40(1)

## Optical properties

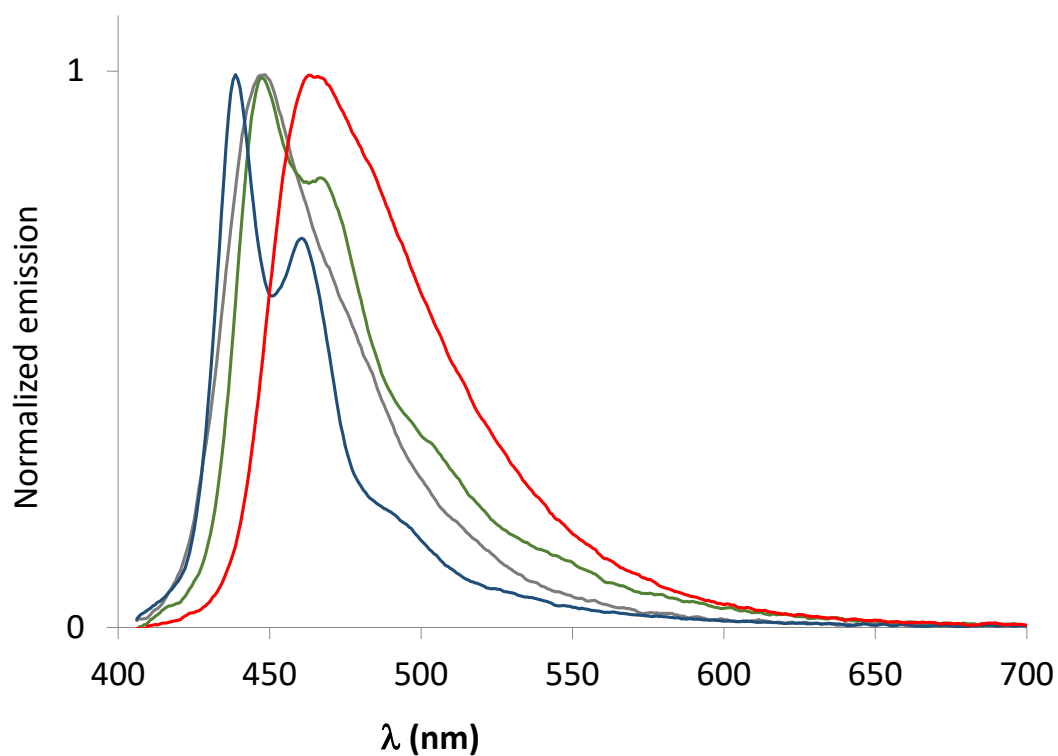


Figure S13: normalized emission in powder of **2a** (grey), **2b** (red), **3** (green), **4** (orange).

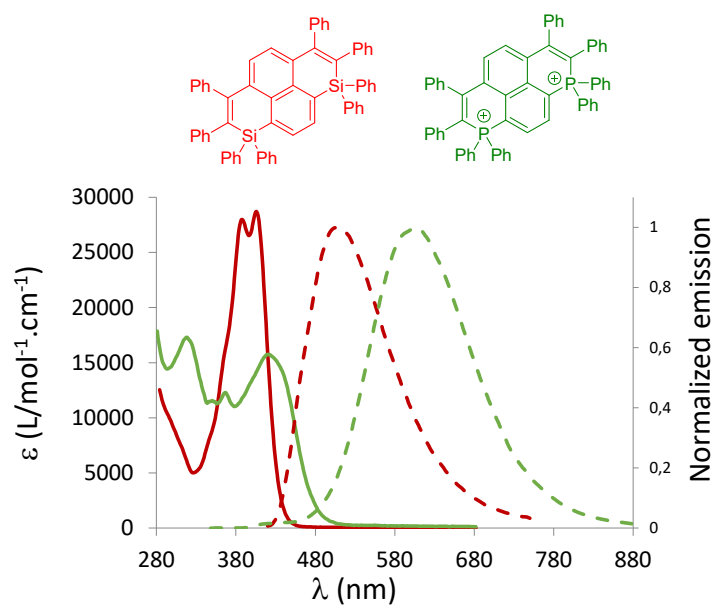
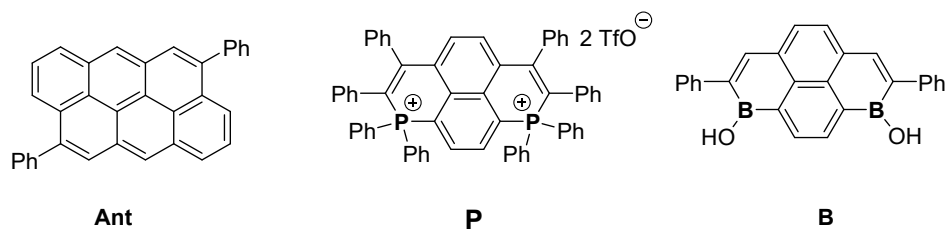


Figure S14: comparison between the absorption (solid line) and emission (dashed line) of **2a** and its corresponding diphosphaperylenium in diluted DCM.

Table S3: optical and redox data of related derivatives



	$\lambda_{\text{abs}}^{\text{a}}$ (nm)	$\lambda_{\text{em}}^{\text{a}}$ (nm)	$E_{\text{ox}}^{\text{b}}$ (V vs Fc)	$E_{\text{red}}^{\text{b}}$ (V vs Fc)
<b>pyrene</b>	338	372	+0,9 V	-
<b>Ant<sup>4</sup></b>	439	442	-	-
<b>P<sup>5</sup></b>	420	606	-	-0,84
<b>B<sup>6</sup></b>	466	586	-	-1.46

<sup>a</sup>In CH<sub>2</sub>Cl<sub>2</sub> (10<sup>-5</sup>M). <sup>b</sup>(c = 10<sup>-3</sup> M) recorded in CH<sub>2</sub>Cl<sub>2</sub> with Bu<sub>4</sub>N<sup>+</sup>PF<sub>6</sub><sup>-</sup> (0.2 M) at a scan rate of 200 mVs<sup>-1</sup>. Potentials vs Fc<sup>+/0</sup>.

## Electrochemical properties

<sup>4</sup> B. K. Shah, D. C. Neckers, J. Shi, E. Forsythe and D. Morton, *J. Phys. Chem. A* **2005**, 109, 7677-7681.

<sup>5</sup> T. Delouche, A. Vacher, E. Caytan, T. Roisnel, B. Le Guennic, D. Jacquemin, M. Hissler and P.-A. Bouit, *Chem. Eur. J.* **2020**, **26**, 8226-8229

<sup>6</sup> J. M. Farrell, C. Mützel, D. Bialas, M. Rudolf, K. Menekse, A.-M. Krause, M. Stolte and F. Würthner, *J. Am. Chem. Soc.* **2019**, **141**, 9096-9104.

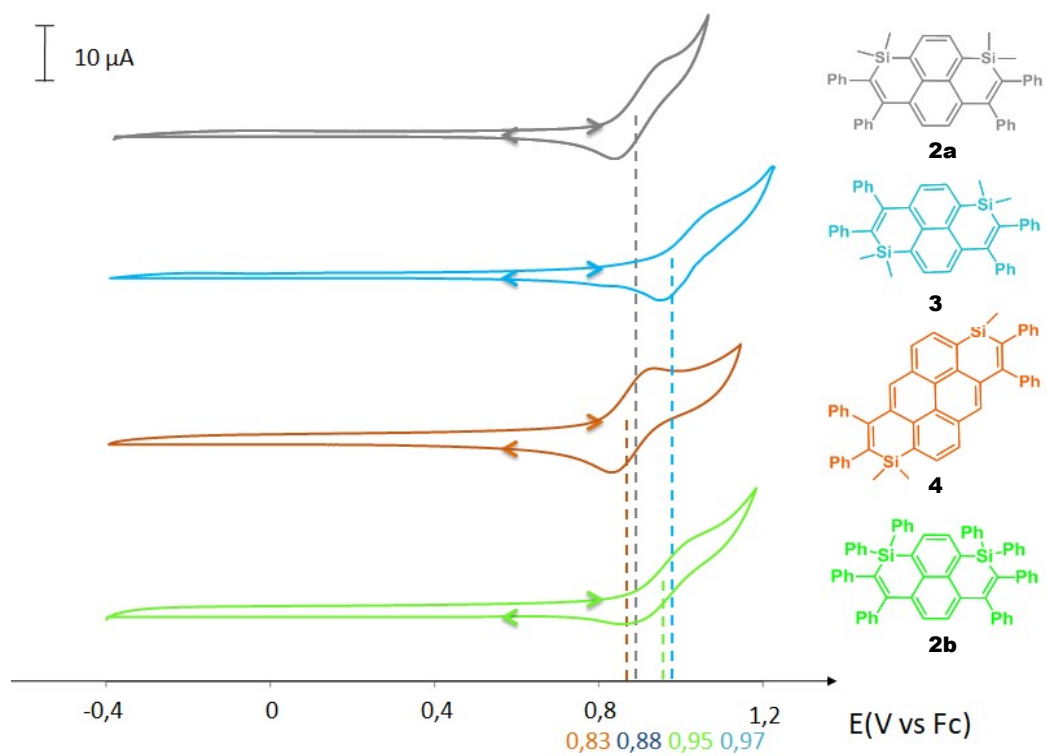


Fig S15: Cyclic voltammograms of **2-4** ( $c = 5.10^{-4}$  M) recorded in DCM ( $\text{Bu}_4\text{NPF}_6$  (0.2 M),  $200 \text{ mVs}^{-1}$ , potentials vs  $\text{Fc}^+/\text{Fc}$ ).

# Theoretical Studies

## 1.1. Computational Details

All theoretical calculations have been performed with the Gaussian16 code.<sup>7</sup> We have applied default algorithms, parameters and convergence thresholds, but for those detailed below. The general protocol applied here follows a series of previous benchmarks performed for organic dyes and we refer the interested readers to these previous assessments for justifications and extra details.<sup>8</sup> First, we have performed ground-state geometry optimizations of all compounds using the M06-2X<sup>9</sup> functional combined with the 6-31G(d) atomic basis set for all atoms. During the force minimization process, the solvent effects (CH<sub>2</sub>Cl<sub>2</sub>) were accounted for using the Polarizable Continuum Model (PCM).<sup>10</sup> Next it was systematically checked, using an analytical determination of the nuclear Hessian, that all structures are true minima of the potential energy surface. The vertical transition energies to the lowest excited-states were determined using Time-Dependent Density Functional Theory (TD-DFT)<sup>11</sup> in combination with the same functional,<sup>6</sup> and a significantly larger basis set, namely 6-311+G(2d,p). During the vertical and energy TD-DFT calculations the solvent effects were accounted for using a combination<sup>12</sup> between the linear-response (LR)<sup>13</sup> and corrected linear-response (cLR)<sup>14</sup> formalisms of PCM and applying the *non-equilibrium* limit. The procedure followed to obtain estimates of the vertical fluorescence energies was very similar, with analytic optimization and vibrational frequencies of the lowest singlet states performed at the PCM(LR,*eq*)-M06-2X/6-31G(d) level, followed by determination of the emission transitions at the PCM(LR+cLR,*neq*)-M06-2X/6-311+G(2d,p) level.

---

<sup>7</sup> M. J. Frisch, et al., Gaussian 16, Rev. A.03, **2016**, Gaussian Inc. Wallingford, CT.

<sup>8</sup> See, e.g., a) B. Le Guennic, D. Jacquemin, *Acc. Chem. Res.*, **2015**, *48*, 530; b) D. Jacquemin, I. Duchemin, X. Blase, *J. Chem. Theory Comput.*, **2015**, *11*, 5340.

<sup>9</sup> Y. Zhao, D. G. Truhlar, *Theor. Chem. Acc.*, **2008**, *120*, 215.

<sup>10</sup> J. Tomasi, B. Mennucci, R. Cammi, *Chem. Rev.* **2005**, *105*, 2999.

<sup>11</sup> C. Adamo, D. Jacquemin, *Chem. Soc. Rev.* **2013**, *42*, 845.

<sup>12</sup> P. M. Vérité, C. A. Guido, D. Jacquemin, *Phys. Chem. Chem. Phys.* **2019**, *21*, 2307.

<sup>13</sup> R. Cammi, B. Mennucci, *J. Chem. Phys.* **1999**, *110*, 9877.

<sup>14</sup> M. Caricato, B. Mennucci, J. Tomasi, F. Ingrosso, R. Cammi, S. Corni, G. Scalmani, *J. Chem. Phys.*, **2006**, *124*, 124520.

## 1.2. Additional results and figures

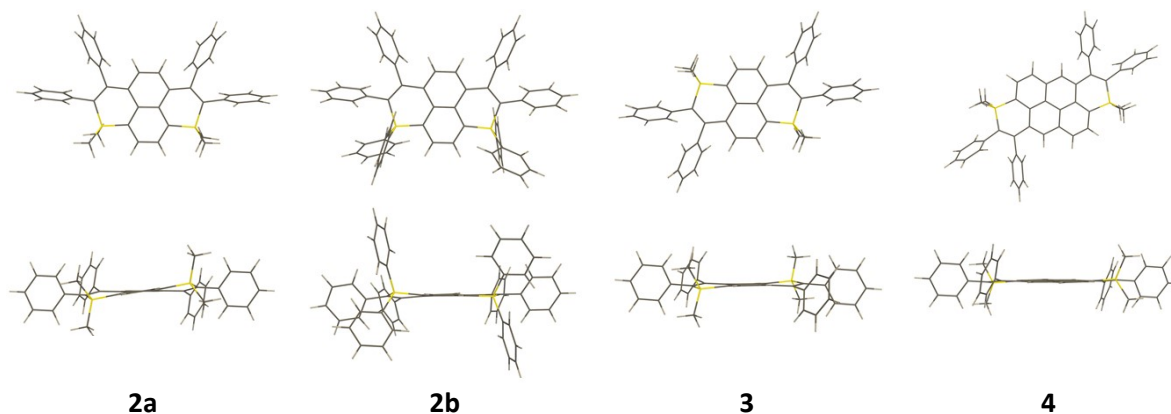


Figure S15: Top and lateral views of the **2-4** as obtained by PCM-DFT optimization.

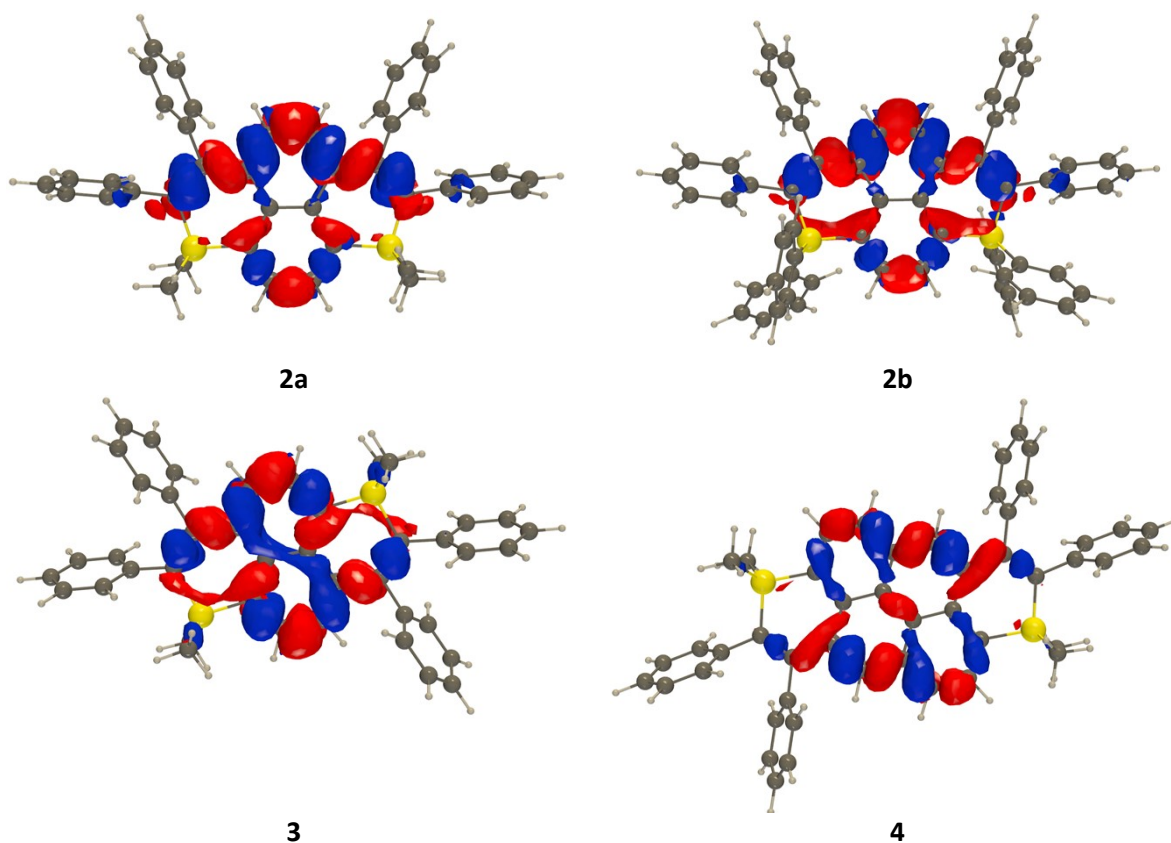


Figure S16: Density difference plots for the lowest transition of **2-4**. The blue and red lobes respectively represent regions of decrease and increase of electronic density (upon absorption). Contour threshold: 0.0008 au.



**Table S4:** Theoretical best estimates for the vertical absorption, vertical emission and 0-0 energies, given in both eV and nm. Note that the two former have no clear experimental counterpart, whereas the latter can be compared to the experimental crossing point of the absorption and emission curves.

	Vert. Abs.		Vert. Fluo.		0-0		
	$\Delta E$	$\lambda$	$\Delta E$	$\lambda$	$\Delta E$	$\lambda_{\text{calc}}$	$\lambda_{\text{exp}}$
<b>2a</b>	3.386	366	2.413	514	2.888	429	421
<b>2b</b>	3.347	371	2.278	544	2.799	442	434
<b>3</b>	3.467	358	2.529	490	3.014	411	410
<b>4</b>	3.433	361	2.825	439	3.057	405	408

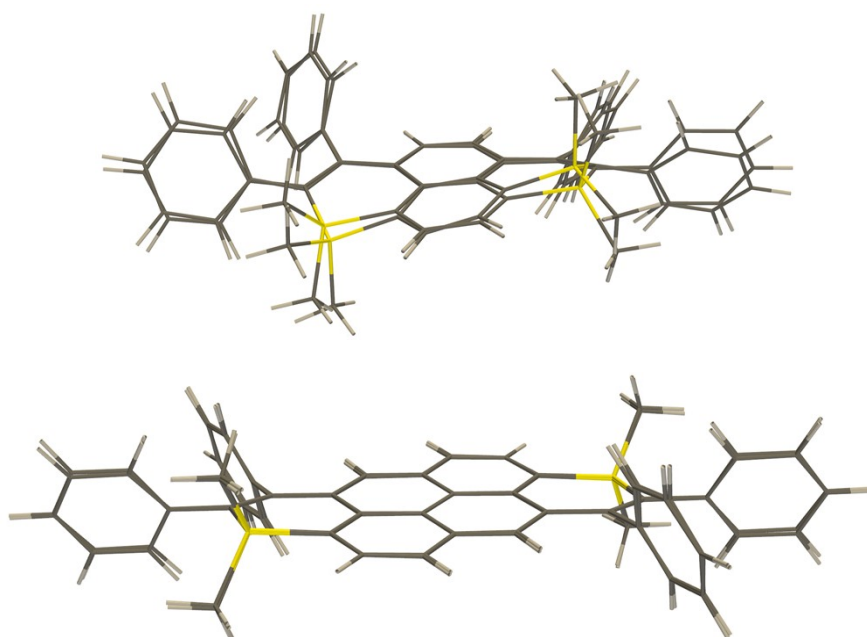


Figure S17: Superposition of the minimal  $S_0$  and  $S_1$  geometries for **2a** (top) and **4** (bottom) as computed by TD-DFT.

## Thermal stability

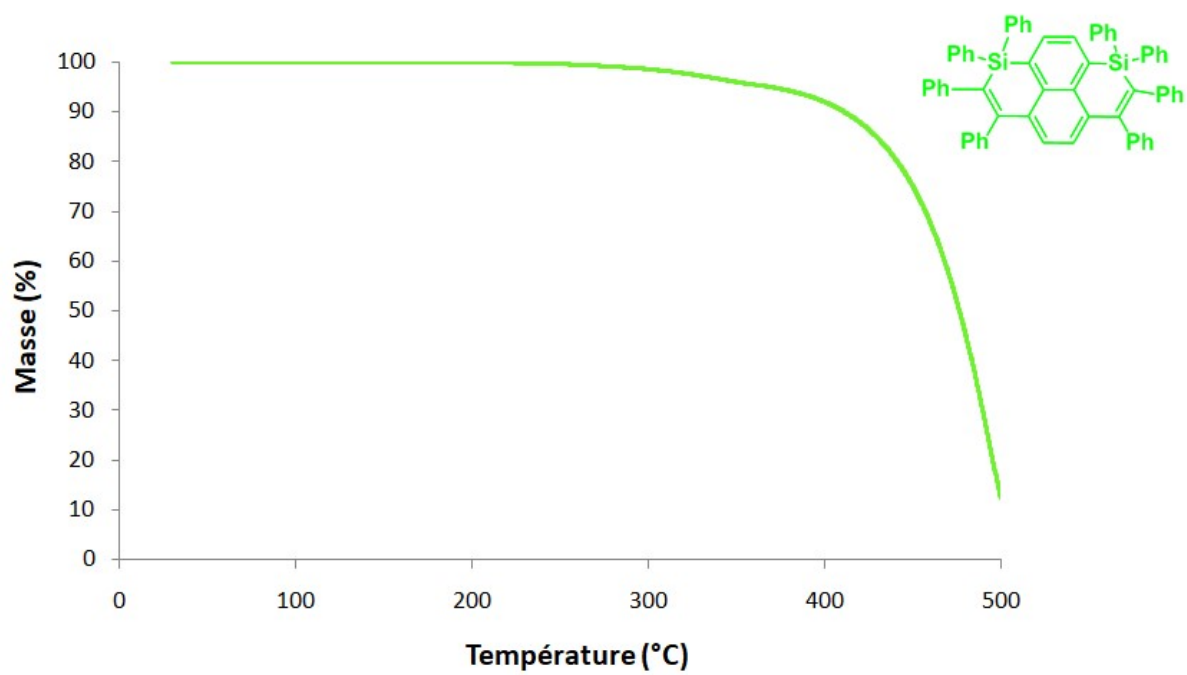


Figure S18: Thermogravimetric analyses (TGA) measurements performed on **2b**

## OLEDs fabrication and characterisation

### Devices prepared by sublimation.

The OLED devices were fabricated onto indium tin oxide (ITO) glass substrates purchased from Xin Yang Technology (90 nm thick, sheet resistance of  $15 \Omega/\square$ ). Prior to organic layer deposition, substrates etching was performed on 1/3 of part the substrates with Zn powder and hydrochloric acid. After that substrate were cleaned by sonication in a detergent solution, rinsed twice in de-ionized water, acetone and then in isopropanol solution respectively each for 15 minutes. After cleaning, substrates were placed inside the vacuum thermal evaporator for chromium/gold ( $\text{Cr}_{15\text{nm}}/\text{Au}_{100\text{nm}}$ ) coating for contacts. Cr/Au deposited substrates were cleaned with isopropanol for 15 minutes under sonication then placed under UV -exposure for 15 minutes and placed all substrates inside the vacuum chamber for deposition of different layers.

The OLEDs stack in device A-E used is: Glass / ITO / CuPc (10 nm) /  $\alpha$ -NPB (40 nm) / TcTa (10 nm) / EML (20 nm) / TPBi (50 nm) / LiF (1.2 nm) / Al (100 nm). Copper II phthalocyanine (CuPc) is used as hole injection layer (HIL), N, N'-Bis-(1-naphthalenyl)- N,N'-bis-phenyl-(1,1'-biphenyl)-4,4'-diamine ( $\alpha$ NPB) and Tris(4-carbazoyl-9-ylphenyl)amine (TcTa) as hole transport layer (HTL), 1,2,2',2''-(1,3,5-Benzinetriyl)-tris(1-phenyl-1-H-benzimidazole (TPBi) as electron transport layer (ETL), lithium fluoride as electron injection layer (EIL) and 100 nm of aluminum as the cathode, respectively. The emitting layer (EML) is a host-guest system of 20 nm thick with 1,3-Bis(*N*-carbazoyl)benzene (mCP) or (4,4'-Bis(*N*-carbazoyl)-1,1'-biphenyl) CBP as the host and molecule **2b** as the guest (doping ratio 0-10% weight). Organic layers were sequentially deposited onto the ITO substrate at a rate of 0.2 nm/s under high vacuum ( $10^{-7}$  mbar). The doping rate was controlled by simultaneous co-evaporation of the host and the dopant. An in-situ quartz crystal was used to monitor the thickness of the layer depositions with an accuracy of 5%. The active area of the devices defined by the Al cathode was  $0.28 \text{ cm}^2$ . The organic layers and the LiF/Al cathode were deposited in a one-step process without breaking the vacuum.

### Devices prepared by solution process

Solution preparation: 2:1 ratio of Poly(9-vinylcarbazole) (PVK:12 mg) and 2-(4-tert-Butylphenyl)-5-(4-biphenylyl)-1,3,4-oxadiazole (OXAD:6 mg) were dissolved in 600  $\mu\text{L}$  of chlorobenzene and 200  $\mu\text{L}$  of chloroform. **2b** (4% and 10%) was then added to the solution.

Device fabrication process: For the etching of the ITO coated glass substrates we followed the same procedure as mentioned in the previous section. Then, Cr/Au substrates were cleaned with isopropanol for 15 under sonication then placed under UV -exposure for 15 minutes. After that, poly(3,4-ethylenedioxythiophene) polystyrene sulfonate (PEDOT: PSS) layer was deposited at 4500 rpm for 40 s and dried at  $120 \text{ }^\circ\text{C}$  for 30 minutes in ambient condition. Then, in glove box EML (PVK\_OXAD\_2b (4% and 10%)) layer was spin coated at 4500 rpm for 40 s and dried at  $150 \text{ }^\circ\text{C}$  for 5 minutes over the PEDOT: PSS layer. Then, the other layers Bathocuproine ( $\text{BCP}_{10\text{nm}}$ ) as hole blocking layer, Tris-(8-hydroxyquinoline) aluminum ( $\text{Alq}_{30\text{nm}}$ ) as electron transfer layer, Lithium fluoride/aluminum ( $\text{LiF}_{1.2\text{nm}}/\text{Al}_{100\text{nm}}$ ) as cathode respectively were deposited by vacuum sublimation.

After deposition, all the measurements were performed at RT and under ambient atmosphere with no further encapsulation of devices. The current–voltage–luminance (I–V–L) characteristics of the devices were measured with a regulated power supply (ACT100 Fontaine) combined with a multimeter (Keithley) and a  $1 \text{ cm}^2$  area silicon calibrated photodiode (Hamamatsu). Electroluminescence (EL) spectra and chromaticity coordinates of the devices were recorded with a PR650 SpectraScan spectrophotometer, with a spectral resolution of 4 nm.

**Devices Architecture:**

**A:** Glass/ITO/CuPc<sub>10nm</sub>/NPB<sub>40nm</sub>/TcTa<sub>10nm</sub>/mCP<sub>20nm</sub>/TPBi<sub>50nm</sub>/LiF<sub>1.2nm</sub>/Al<sub>100nm</sub>

**B:** Glass/ITO/CuPc<sub>10nm</sub>/NPB<sub>40nm</sub>/TcTa<sub>10nm</sub>/mCP:**2b(X%)**<sub>20nm</sub>/TPBi<sub>50nm</sub>/LiF<sub>1.2nm</sub>/Al<sub>100nm</sub>

**C:** Glass/ITO/CuPc<sub>10nm</sub>/NPB<sub>40nm</sub>/TcTa<sub>10nm</sub>/CBP<sub>20nm</sub>/TPBi<sub>50nm</sub>/LiF<sub>1.2nm</sub>/Al<sub>100nm</sub>

**D:** Glass/ITO/CuPc<sub>10nm</sub>/NPB<sub>40nm</sub>/TcTa<sub>10nm</sub>/CBP:**2b(X%)**<sub>20nm</sub>/TPBi<sub>50nm</sub>/LiF<sub>1.2nm</sub>/Al<sub>100nm</sub>

**E:** Glass/ITO/PEDOT: PSS<sub>40nm</sub>/PVK\_Oxad (12:6): **2b(X%)**<sub>80nm</sub>/CBP<sub>10nm</sub>/Alq<sub>3</sub><sub>20nm</sub> LiF<sub>1.2nm</sub>/Al<sub>100nm</sub>

Table S4: Device parameters

Device Type	Doping Rate (%)	Von (V) ± 0.2 V	EQE (%)	Current efficiency (Cd/A)	Power efficiency (lm/W)	CIE (x; y)	Max brightness (cd/m <sup>2</sup> ) @ (mA/cm <sup>2</sup> )
<b>A</b>	Pure mCP	4.4	0.83	0.77	0,29	0.207;0.202	776@ ~(200-250)
<b>B</b>	1.7	4.2	1.13	1.47	0.58	0.177;0.214	1104@250
<b>B</b>	4	4	1.03	1.59	0.63	0.177;0.247	1177@250
<b>B</b>	10	4.3	0.97	1.72	0.65	0.188;0.297	1238@ ~(180-250)
<b>C</b>	Pure CBP	4.18	1.18	0.57	0.26	0.193; 0.144	904 @250
<b>D</b>	1.5	3.57	1.66	2.47	1.2	0.167; 0.223	1560 @250
<b>D</b>	2	3.27	1.69	2.71	1.29	0.167; 0.235	1695 @250
<b>D</b>	4	3.75	1.48	2.8	1.23	0.176; 0.272	1837 @250
<b>D</b>	6	3.49	1.5	2.95	1.47	0.178; 0.301	2054 @300
<b>D</b>	10	3.78	1.43	3.03	1.33	0.191; 0.339	2494 @300
<b>E</b>	4	4.99	0.84	1.64	0.43	0.185; 0.291	894 @100-120
<b>E</b>	10	5.13	0.98	1.72	0.42	0.195; 0.317	839 @100

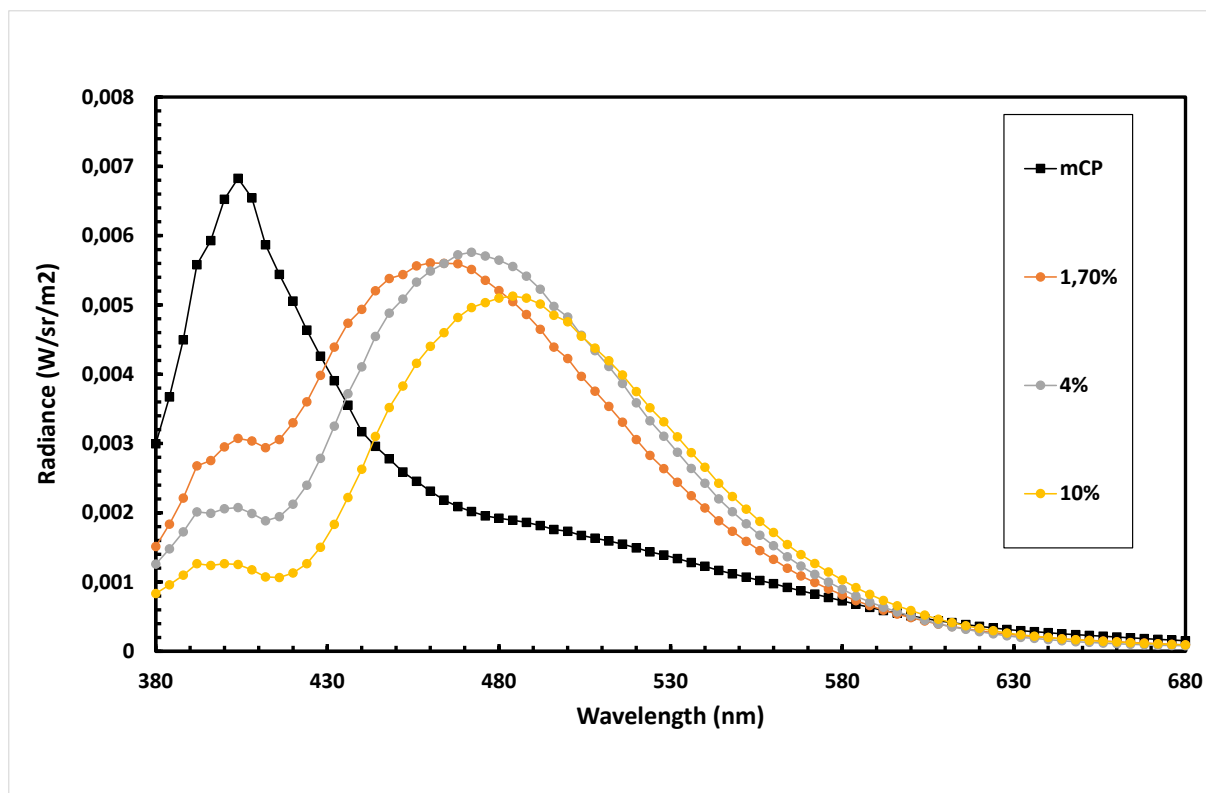


Fig. S19. Electroluminescence spectra recorded at  $30 \text{ mA/cm}^2$  for **2b** at different doping rates in mCP.

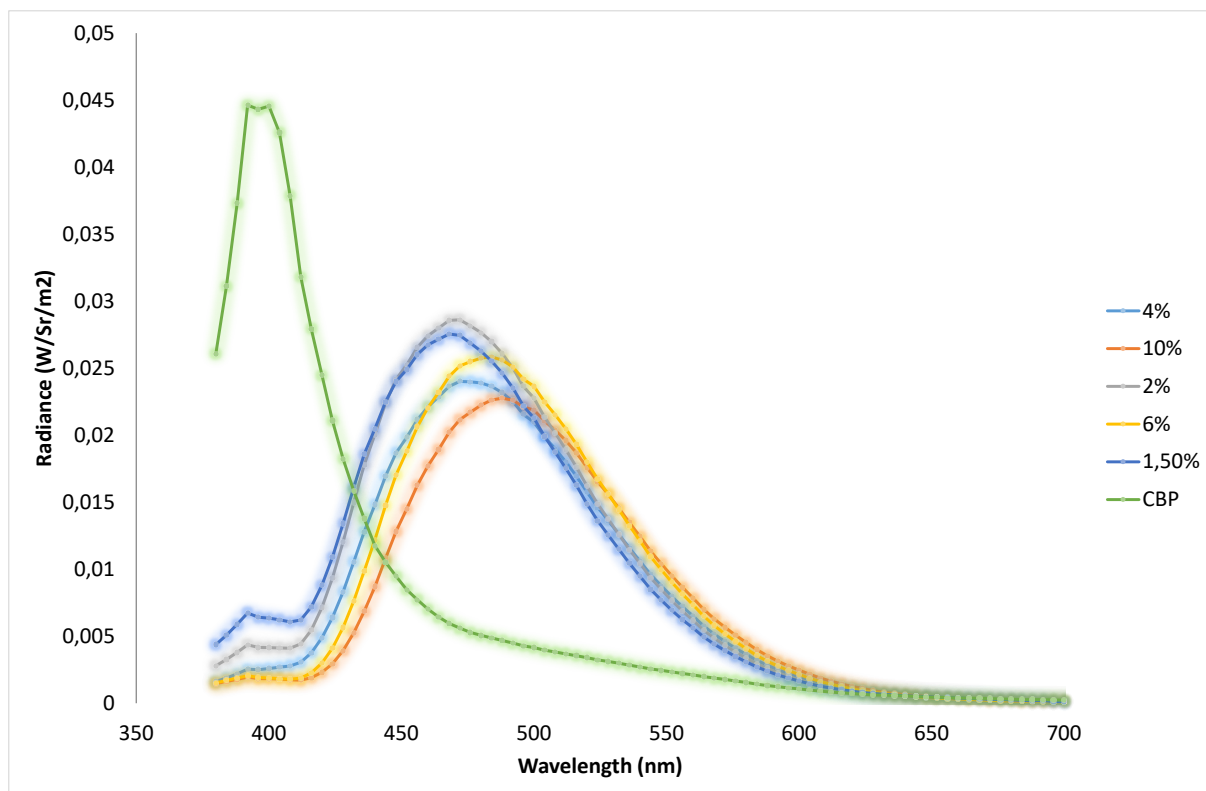


Fig. S20. Electroluminescence spectra recorded at  $30 \text{ mA/cm}^2$  for **2b** at different doping rates in CBP.

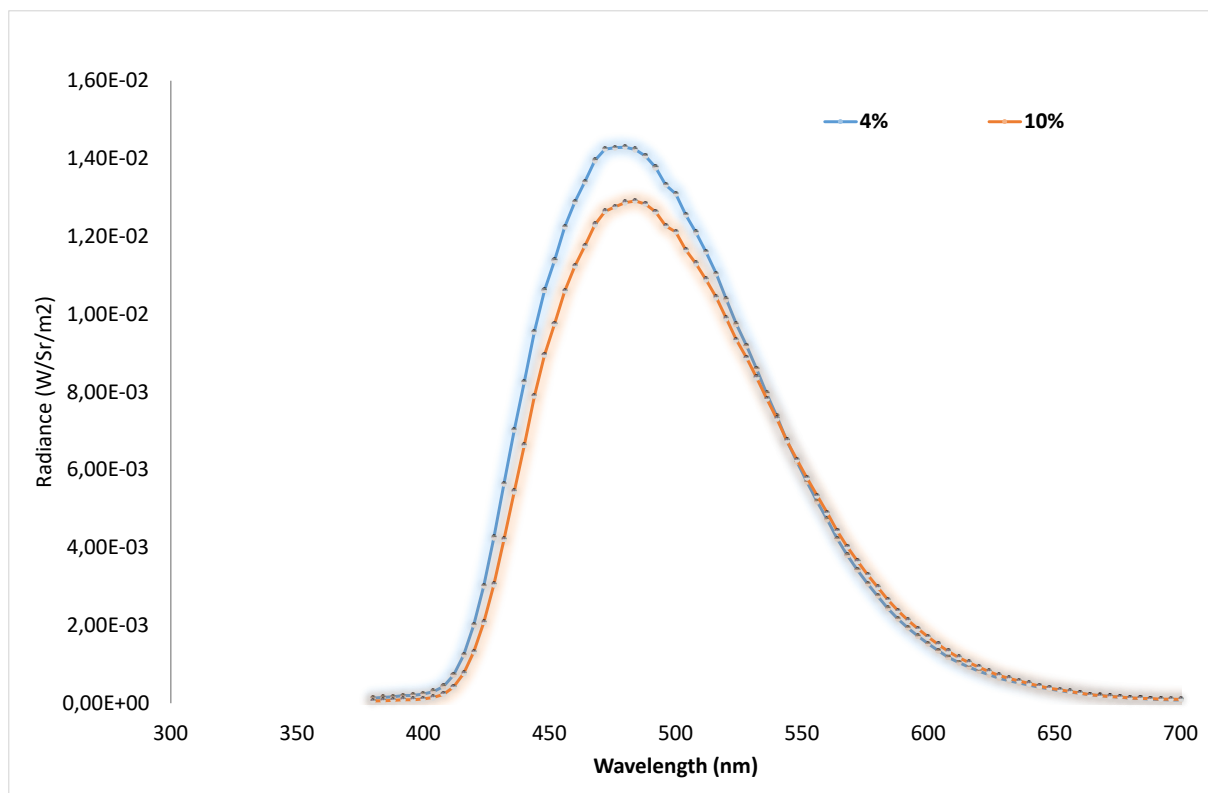


Fig. S21. Electroluminescence spectra recorded at 30 mA/cm<sup>2</sup> for **2b** at different doping rates in PVK-Oxadiazole (2:1).